Understanding the Unusual Track of Typhoon Lionrock (2016)

MENGYUAN MA,[a] MELINDA S. PENG,[b] TIM LI,[c,d,a] AND LIJUAN WANG[a]

[a] *Key Laboratory of Meteorological Disaster, Ministry of Education (KLME)/Joint International Research Laboratory of Climate and Environment Change (ILCEC)/Collaborative Innovation Center on Forecast and Evaluation of Meteorological Disasters (CIC-FEMD), Nanjing University of Information Science and Technology, Nanjing, China*
[b] *University of Colorado, Colorado Springs, Colorado*
[c] *International Pacific Research Center, University of Hawai'i at Mānoa, Honolulu, Hawaii*
[d] *Department of Atmospheric Sciences, School of Ocean and Earth Science and Technology, University of Hawai'i at Mānoa, Honolulu, Hawaii*

ABSTRACT: The unusual movement of Typhoon Lionrock (2016) that posed great challenges for operational numerical predictions was investigated. Analysis of the steering flow at different levels shows that Lionrock's southwestward motion before 25 August was mainly controlled by the upper-level steering, and the dominant steering shifted to lower levels as the storm turned northeastward abruptly afterward. To examine the influence of the environmental flow on this major turning of Lionrock, three numerical simulations are conducted using the Weather Research and Forecasting (WRF) Model with different starting times. The study indicates that the initial southwestward movement of Lionrock is attributed to the westward extension of the mid- to upper-level subtropical high, and the later turning to northeast is caused by the low-level southwesterly flow associated with the monsoon gyre northeast of Lionrock. In an experiment in which the monsoon gyre is removed from the initial and boundary fields, Lionrock continues its southwestward movement without turning northeastward. This result suggests that the transition of the steering from high to low levels plays a crucial role in the major turning of Lionrock. More sensitivity experiments with modifications of the initial and/or the boundary conditions indicate a low predictability of Lionrock's major turning.

KEYWORDS: Storm tracks; Tropical cyclones; Numerical weather prediction/forecasting

1. Introduction

The western North Pacific (WNP) is a region with frequent tropical cyclones (TCs), accounting for about one-third of global TCs each year (Lee et al. 2012; Li and Hsu 2018). Among them, landfalling TCs usually have widespread impacts on eastern Asia, with disasters causing fatalities and huge economic losses. Prediction of TC tracks and intensities remains as a serious and challenging problem despite improvements in recent decades (DeMaria et al. 2014).

Previous studies have indicated that many factors can affect the track of a TC. Many studies have revealed that the large-scale environmental flow is the main factor that affects the TC movement (Kasahara 1957, 1960; George and Gray 1976; Holland 1983, 1984; Carr and Elsberry 1990: Wu and Emanuel 1995a,b). Chan and Gray (1982) indicated that TC movement is sensitive to its surrounding large-scale flow, and has a good correlation with the averaged midtroposphere winds within 5°–7° radius from the TC center. Holland (1984) further suggested that the deep-layer steering flow represented by the vertically averaged horizontal wind field between 850 and 300 hPa correlates well with the storm motion. However, in some individual cases, the steering flow may have a large variation with height (George and Gray 1976; Torn et al. 2018). Velden and Leslie (1991) demonstrated that the environmental steering flow corresponds better with the TC motion when the depth of the steering layer is constructed as intensity dependent.

Complex interactions between a TC and its surroundings can result in large forecast errors and pose great challenges on operational predictions for TCs. In previous studies, the subtropical ridge and the midlatitude synoptic waves are often mentioned as main factors in modulating tropical cyclone movements and intensity changes (Bosart et al. 2000; Harr et al. 2000; J.-H. Chen et al. 2009; Sun et al. 2015). Wu et al. (2007) showed that the expansion or contraction of the subtropical ridge in the WNP is crucial to the TC recurvature. Specifically, J.-H. Chen et al. (2009) indicated that the typhoon (TC in WNP) motion is related to the steering flow from the subtropical high. In addition, the movement of a TC is sensitive to its position relative to approaching midlatitude troughs (Hanley et al. 2001; Peng et al. 2007; Wu et al. 2009). The monsoon circulation also plays an important role modulating the motion and structure of TCs in the WNP (Harr and Elsberry 1991). In general, tropical cyclones are often embedded in the large monsoon circulation in the WNP (Lau and Lau 1990, 1992; Chang et al. 1996; Straub and Kiladis 2003). T. C. Chen et al. (2009) suggested that when there is a strong monsoon trough, the associated flow is more likely to cause the TC to recurve, while straight-moving TCs are associated with a strong subtropical anticyclone extended to the west. Lander (1996) explained the relationship between TC motion and monsoon trough orientation from a synoptic perspective. When the axis of the monsoon trough is in a reversed orientation (southwest–northeast), a TC within it has a northward moving trend. Binary interactions between two storms, the Fujiwhara effect, can also affect the TC movement (Fujiwhara 1921, 1923; Brand 1970; Dong and Neumann 1983; Lander
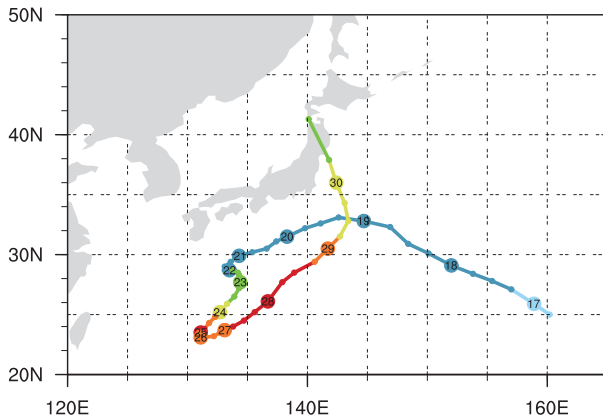
FIG. 1. The JTWC best track of Lionrock from 1800 UTC 16 Aug to 1200 UTC 30 Aug 2016. Different colors represent different TC intensity. TC strength is divided into maximum wind speed of 18–24 m s^{-1} (blue), 25–32 m s^{-1} (green), 33–41 m s^{-1} (yellow), 42–51 m s^{-1} (orange), and greater than or equal to 52 m s^{-1} (red).

and Holland 1993; Carr and Elsberry 1998). Studies have shown that large-scale monsoon gyre interaction with a typhoon can also lead to a sudden change of the TC motion (Carr and Elsberry 1995; Liang et al. 2011; Bi et al. 2015; Liang and Wu 2015; Ge et al. 2018).

In the WNP, some typhoons experience significant track changes from mainly westward to move northward, followed by a northeastward track (a recurvature) and then undergo an extratropical transition. Lionrock (2016) is a unique case that started in the subtropical region with a big cyclonic looping motion in the early stage. The mainly southwestward motion since 19 August was followed by a sudden northeast turn around 25 August 2016 (Fig. 1), where most operational numerical models failed to predict its unusual turn at the correct time (Fig. 2). When it finally made landfall, Lionrock brought extreme precipitation and flooding to the coastal regions in eastern Asia, especially Japan. Some studies have focused on investigating Lionrock's second turn from a northeast movement to northwestward around 29 August and have discussed the interaction between the storm and the large-scale circulation (Dzung and Yamada 2017; Bosart et al. 2018; Torn et al. 2018; Wada and Oyama 2018). The objective of this study is to understand mechanisms behind Lionrock's sudden northeastward turn at around 25 August 2016.

The rest of the paper is organized as follows. Section 2 provides a brief overview of the history for Typhoon Lionrock. In section 3, we describe the model and dataset used, and the experiments design for the simulation of Lionrock. Section 4 discusses the steering flows at different levels related to Lionrock's movement. In section 5, we investigate mechanisms responsible for Lionrock's sudden movement. The predictability of Lionrock's sudden turn is examined in section 6. Finally, the conclusions and discussion are presented in section 7.

2. Overview of Lionrock life cycle

Typhoon Lionrock is the tenth tropical cyclone in the western Pacific in 2016. The beginning of its life cycle can be traced back
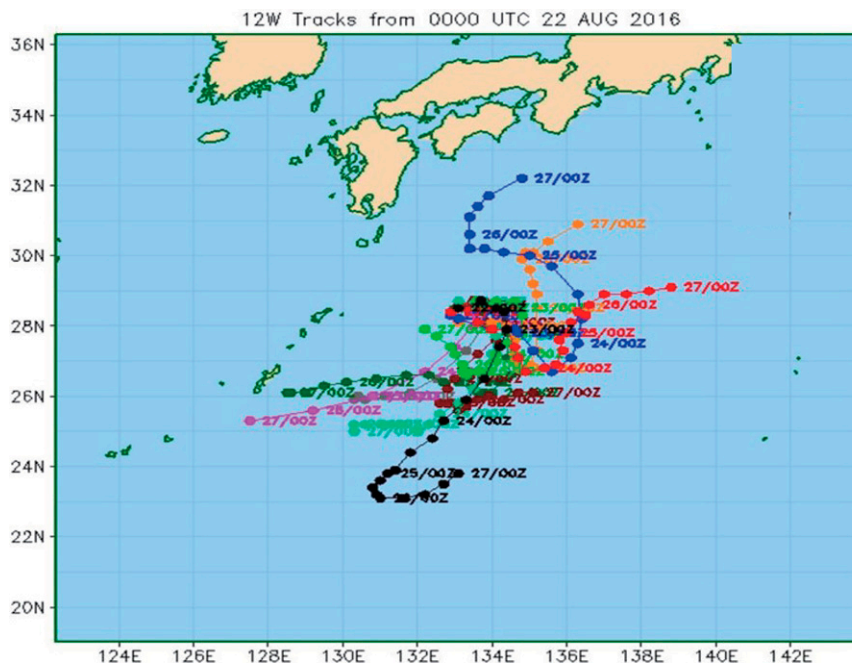

FIG. 2. Different model forecast tracks of TC Lionrock from 0000 UTC 22 Aug to 0000 UTC 27 Aug 2016. The black line represents the observation track of TC Lionrock. The identifications of individual model have been removed. Source of the plot: https://www.nrlmry.navy.mil/coamps-web/web/tc.
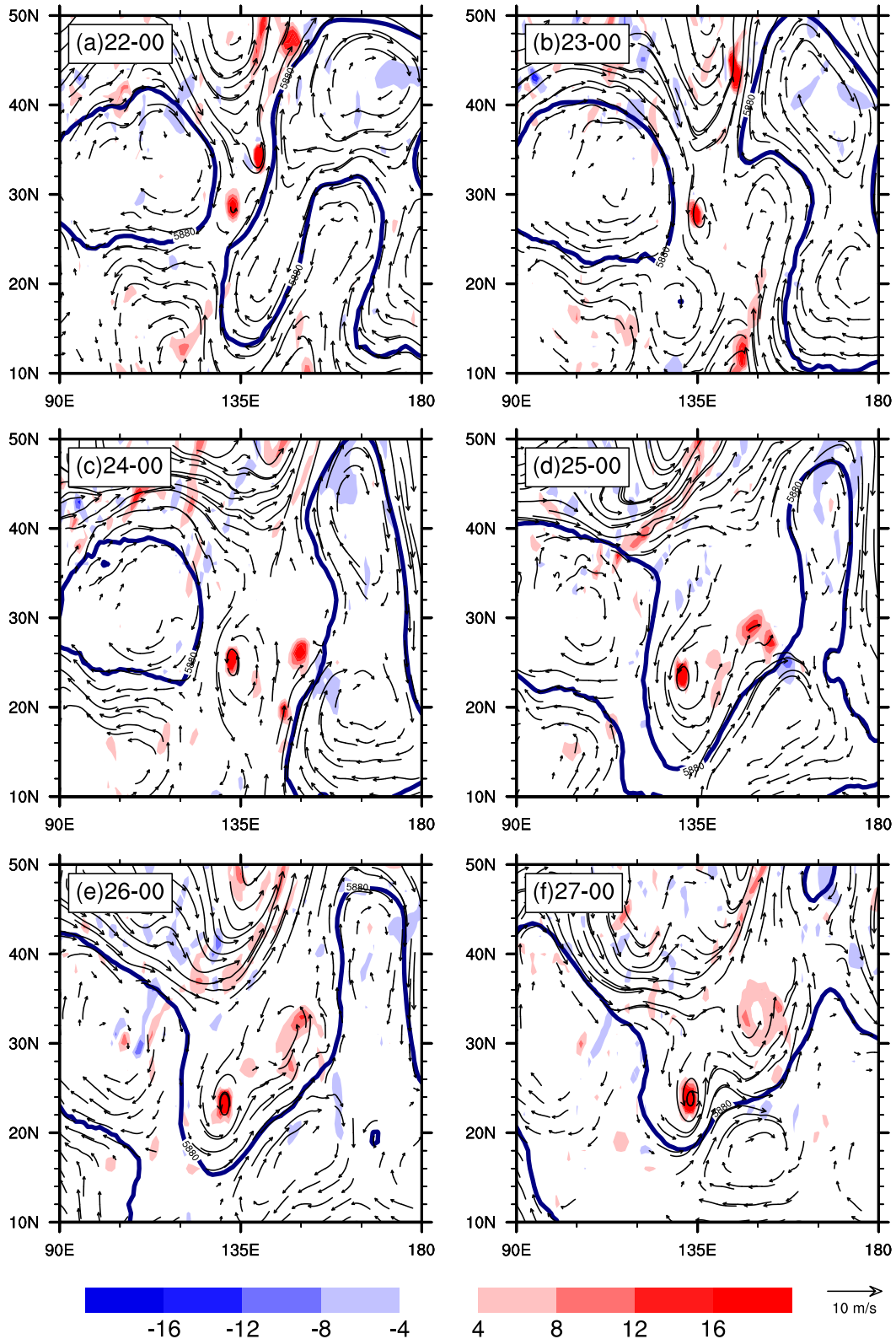
FIG. 3. Observed 5880-gpm geopotential height (contour) and wind field (vector; m s^{-1}) at 500 hPa, and vorticity (shaded; 10^{-4} s^{-1}) at 850 hPa from (a) 0000 UTC 22 Aug to (f) 0000 UTC 27 Aug 2016 at 24-h intervals.
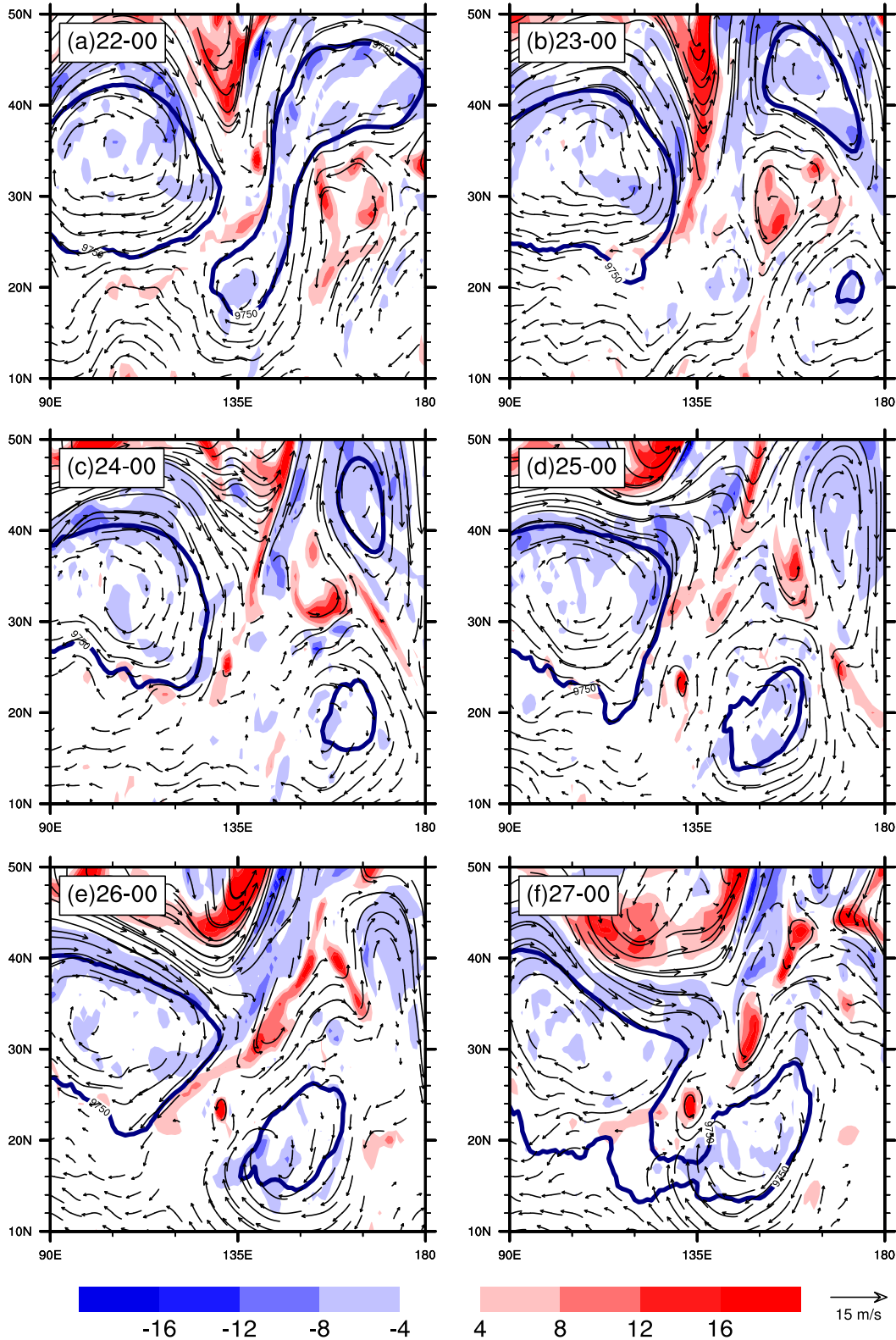
Fig. 4. Observed 9750-gpm geopotential height (contour), wind field (vector; m s^{-1}), and vorticity (shaded; 10^{-4} s^{-1}) at 300 hPa from (a) 0000 UTC 22 Aug to (f) 0000 UTC 27 Aug 2016 at 24-h intervals.

to a subtropical cyclonic disturbance that appeared around 160°E on 15 August 2016. Subsequently, its track began to move northwestward, and it became a tropical storm. After slow development for nearly 4 days, its central pressure reached 996 hPa, and the tropical storm was named Lionrock. Lionrock took on a tropical transition (Davis and Bosart 2004) and moved along a broad counterclockwise track (Fig. 1). It was upgraded to typhoon category by the Joint Typhoon Warning Center (JTWC) at 1800 UTC 23 August. The cyclone made a major turn from a southwestward movement to northeastward at 136°E around 25–26 August. Lionrock reached its peak intensity with a central minimum pressure of 933 hPa and maximum wind speed of 62 m s^{-1} at 0000 UTC 28 August. Then, the cyclone underwent an extratropical transition. While merging with an extratropical cyclone, Lionrock made landfall over the northern Japan and further produced catastrophic flooding in a wide area of East Asia subsequently. It caused over 500 deaths, and over 1 billion dollars in serious damage (Podlaha et al. 2016). Lionrock was also recorded as the first TC landfalling on the Pacific side of northern Japan since 1951 when the statistics of tropical cyclones started (Wada and Oyama 2018).

The two transitions of Lionrock in and out of the tropics are associated with its unusual and complex track. The most striking track change is from being southwestward to being northeastward within a day between 25 and 26 August. Most operational TC forecast models failed to predict the track change correctly at this critical time (Fig. 2). Nearly all of the operational models predicted Lionrock to either continue moving to the southwest or turn to the northeast prematurely.

As stated in the introduction, previous studies indicated that the TC track may be affected by environmental flow at different levels. Figure 3 displays the evolution of the geopotential height and the wind field at 500 hPa, and vorticity at 850 hPa from 22 to 27 August using the National Centers for Environmental Prediction Final Analysis (NCEP FNL analysis). The largest vorticity is associated with the storm center in each panel and the subtropical high system is marked by the blue contour of 5880 geopotential meter (gpm). During the first three days, Lionrock is sandwiched between the two subtropical high systems on its west and east side. Lionrock seems to be affected more by the anticyclone on its west side, with a northerly flow impinging on Lionrock at 500 hPa. The subtropical high to the eastern side of Lionrock continues to extend westward, and finally on 25 August, the anticyclones on both sides merge south of Lionrock. Meanwhile, a strong southwest flow appears to the southeast of Lionrock. It is worth noting that Lionrock started to loop back after 25 August. Figure 4 shows the evolution of the wind field and geopotential height at 300 hPa at the same time as in Fig. 3. The blue contour represents 9750 gpm. The wind field at 300 hPa shows that Lionrock is affected by the northerly wind associated with the anticyclone on the Lionrock's west side on 22–25 August (Fig. 4). Both Figs. 3 and 4 display an upper-level trough that separates the two anticyclones that are to the east and west of Lionrock, thereby inducing a southwestward motion of Lionrock before 25 August. Beyond that, the anticyclone to Lionrock's southeast gradually strengthens
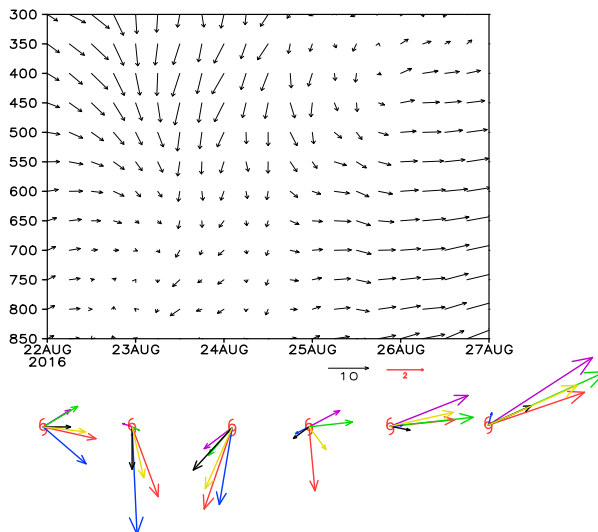

FIG. 5. Time–vertical pressure level (hPa) cross section of steering flow (m s^{-1}) area-averaged over a 500 km × 500 km box centered on the Lionrock center. The vectors below the time axis are the steering flow at 850 hPa (purple), 700 hPa (green), 500 hPa (red), 300 hPa (blue), vertically averaged (from 850 to 300 hPa, yellow), and Lionrock's translation speed (black) from 22 to 27 Aug 2016.

and connects to the anticyclone to the storm's west to form a large trough where Lionrock resides and Lionrock is affected by the southwesterly wind from this trough. The influence of the environmental flow on the movement of Lionrock will be investigated in section 4 with steering vectors computed at different levels.

3. The model and experiment design

a. Model configuration

This study investigates the mechanism behind the sharp turn of Lionrock around 25 August. The numerical model used is version 3.7.1 of the Advanced Research core of the Weather Research and Forecasting (WRF-ARW) Model (Skamarock et al. 2008). Three two-way nested domains are configured. The outer domain is centered on the initial position of the storm at 30°N, 135°E, covering an area of about 8000 km by 6000 km, which is large enough to allow proper representation of the environmental field. The two inner domains move with the storm during the integration. The horizontal grid sizes are 27, 9, 3 km in each domain and the mesh sizes are 320 × 300, 301 × 301, 361 × 361, respectively. There are 47 vertical levels with the model top at 10 hPa. The NCEP FNL analysis (Kalnay et al. 1996) is used to provide the initial and lateral boundary conditions for our simulations. The model physics include the WSM 6-class cloud microphysics scheme (Hong and Lim 2006), the Dudhia shortwave radiation scheme (Dudhia 1989), and the Rapid Radiative Transfer Model (RRTM) for longwave radiation (Mlawer et al. 1997). The Yonsei University (YSU) planetary boundary layer scheme (Hong et al. 2006), the Unified Noah land surface model (Tewari et al. 2004), and Monin–Obukhov surface-layer scheme
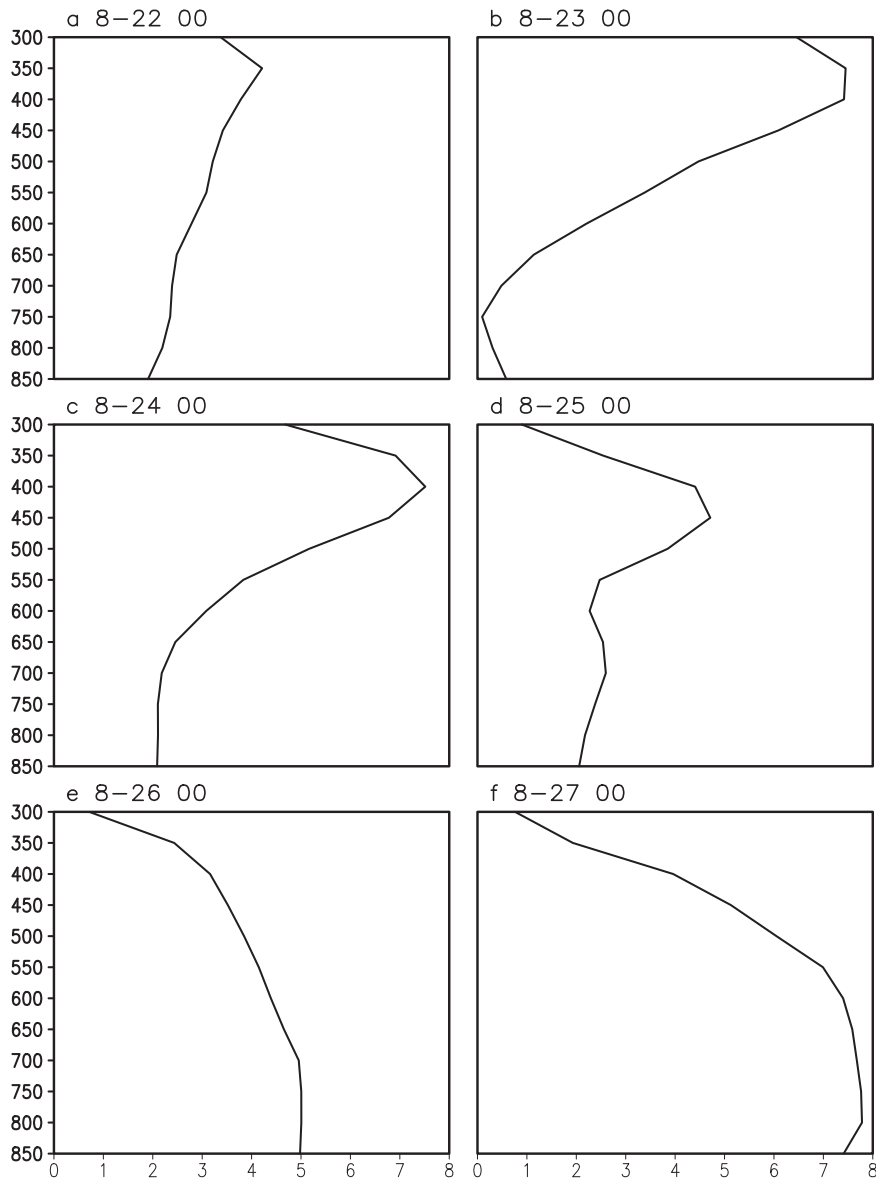
FIG. 6. Vertical profiles of horizontal area-averaged (500 km × 500 km) magnitude of the steering flow (m s^{-1}) from reanalysis.

(Beljaars 1994) are used in all three domains. The Kain–Fritsch convective scheme (Kain and Fritsch 1993) is only used in the outermost and middle meshes.

b. Experimental design

The main purpose of this study is to understand the mechanism behind the sharp turn of Lionrock around 25–26 of August. Three simulations are conducted. The first simulation (SM22) starts at 0000 UTC 22 August 2016 and integrates for 5 days. It starts 3 days before the major turn of Lionrock and this is the time when many operational numerical models were not able to predict the track of Lionrock accurately. The second and the third experiment start at 0000 UTC 23 August

(SM23) and at 0000 UTC 24 August 2016 (SM24), respectively, and are closer to the turning time progressively. Initialized with different time can shed lights on how the simulated environments evolve with different lead times and allow us to examine the reason behind different behavior of Lionrock.

4. The relationship between the steering flow and Lionrock's movement

Before analyzing the numerical simulations to explore mechanisms that affect Lionrock's movement, we examine the steering flow at different vertical levels using the reanalysis data and relate them to the wind and height fields
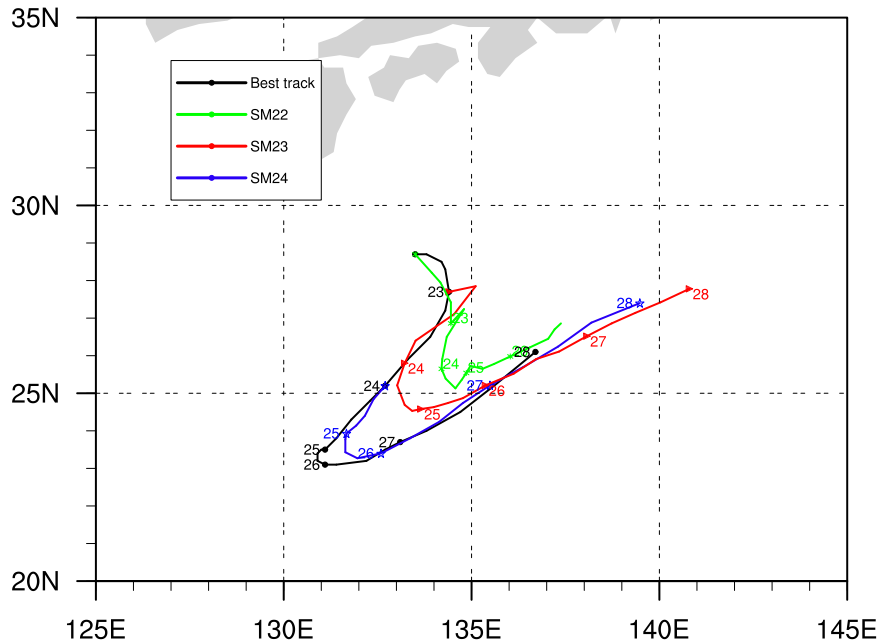
FIG. 7. The JTWC best track (black) of Lionrock and simulated tracks from SM22 (green), SM23 (red), and SM24 (blue).

presented in Figs. 3 and 4. Many previous studies indicated that a good parameter related to the movement of TC is the steering flow across the TC center that represents the asymmetrical flow generated by the large-scale environmental circulation (Kasahara 1957; Holland 1983; Fiorino and Elsberry 1989). Holland (1984) defined the mass-weighted 800–300-hPa vertical averaged wind fields within 6° latitude radius as the representation of the environmental flow steering the cyclone. Features with different time scales are interdependent with the TC movement (Lander and Holland 1993; Carr and Elsberry 1995; Yang et al. 2015). Torn et al. (2018) suggested that the steering flow consists if a multilevel integrated wind fields, with their associated uncertainty.

Instead of looking at the column-integrated steering flow as in most studies, we examine the steering flows at selected significant vertical levels averaged within a radius of 500 km from the TC center. Figure 5 shows the evolutions of the steering flows at different levels from 850 to 300 hPa between 22 and 27 August computed from the NCEP reanalysis. The wind vector below the horizontal time axis represents the speed and direction of the steering flow at several specific pressure levels and the black vector is the TC movement from the best track data. The yellow arrow represents the steering flow vertically averaged from 850 to 300 hPa. Comparing the yellow and black arrows shows that Lionrock's movement is mostly consistent with the vertically averaged steering flow with a smaller angle difference (Chan and Gray 1982). However, near the critical turning time on 25 August, the TC movement speed is very small and the deviation from the averaged steering vector is large, suggesting a large uncertainty at the time. During the period when Lionrock moves

south-southwestward between 0000 UTC 23 August and 0000 UTC 25 August, the directions of the upper-level steering flow above 500 hPa correspond better with the storm motion, indicating an upper-level control of the environment on the movement of Lionrock. The dominating level of the steering flow gradually shifts from upper levels to lower levels when Lionrock turns northeastward on 25–26 August. For example, as can be seen from the arrows below (Fig. 5), the blue (300 hPa) and red (500 hPa) arrows have strong wind speeds before 24 August and are consistent with the actual TC direction. At 0000 UTC 25 August, the 850-hPa (purple arrow) and 700-hPa (green arrow) steering wind speeds begin to increase gradually, although the 500-hPa steering
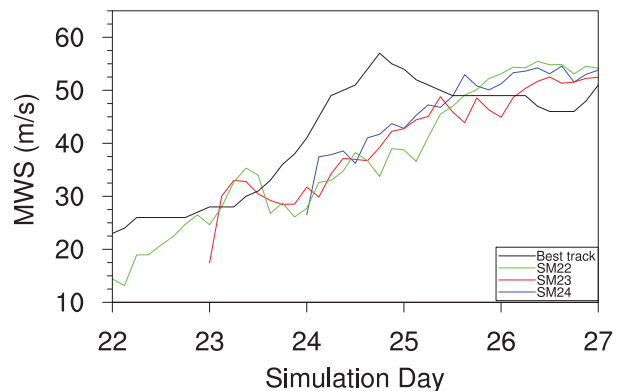

FIG. 8. Time series of the MWS at 10-m height from the best track data (black) and SM22 (green), SM23 (red), and SM24 (blue). The x axis is the calendar day in August 2016.
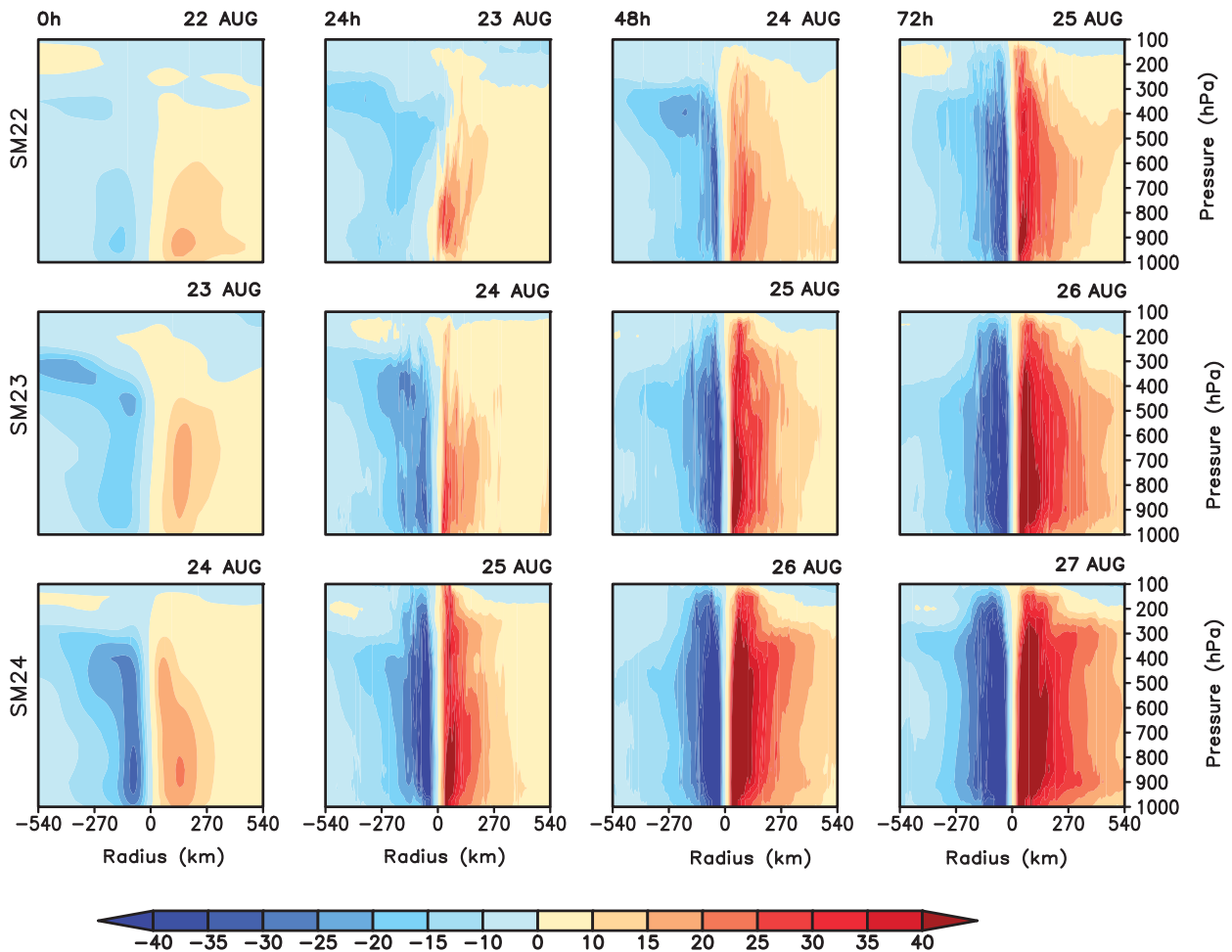
FIG. 9. The vertical cross section of meridional wind across the center of Lionrock in the east–west direction from 1000 to 100 hPa for the SM22, SM23, and SM24 experiments.

flow is still the largest at this time. The major shift occurs between 0000 and 1200 UTC 25 August when the upper-level northerly steering weakens while the lower-level westerly steering strengthens. By 26 August, the lower-level steering flow completely dominates. The time of the transition from the upper-level steering control to the lower-level steering control corresponds exactly to the timing of the turning point of Lionrock. This phenomenon can also be seen more clearly in Fig. 6. Before the turn occurred, the maximum steering flow is located between 450 and 350 hPa from 22 to 25 August. After that, the steering flow at the lower level gradually enhances, which steers the storm northeastward (Fig. 1). This analysis is consistent with the evolution of the environmental fields associated with Lionrock discussed in section 2 and indicates that the sudden track change of Lionrock is a response to the change of the dominating steering level in the vertical. Wu and Wang (2000) proposed that the potential vorticity tendency (PVT) budget is useful to diagnose the TC motion. We conducted the budget of the wavenumber-1 component of PVT and it indicates that the PVT tendency is dominated by the horizontal advection term. In other words, the movement

of Lionrock is controlled by the environmental flows in this case (figure not shown).

5. Influence of the environment on the track of Lionrock

As shown in section 4, the steering flows at different vertical levels have different effects on the TC track at different times. To identify the environmental features that caused Lionrock's sudden turn, further analyses are conducted with the numerical simulations.

The tracks of Lionrock in the three simulations starting at different times with one day apart are plotted in Fig. 7. It is clear that the simulated track in SM24 is closest to the observed track and the time of the turn is also the most accurate, while the simulated tracks are less accurate in SM22 and SM23 and is the worst in SM22. As the forecast lead time increases, Lionrock turns to the northeast too early and the simulated track is too far to the north and east of the actual track. While the current study focuses on the track, the accuracy of the simulated TC intensity is also examined to possibly help understanding the track change. Figure 8 shows the time
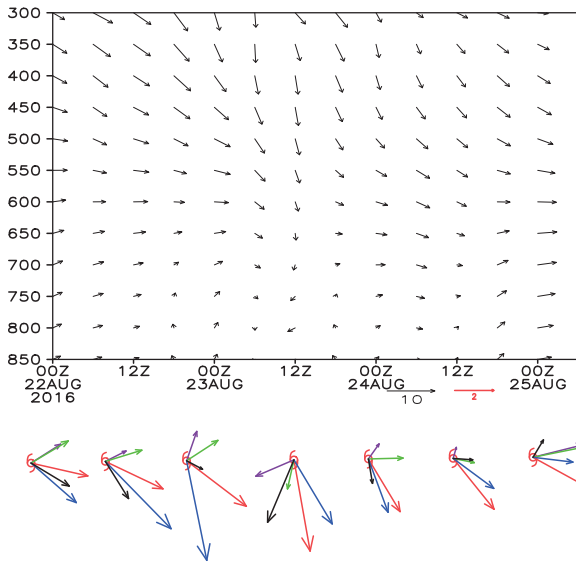
FIG. 10. Time–vertical pressure level (hPa) cross section of steering flow (m s^{-1}) area averaged over a 500 km × 500 km box centered on the TC center. The vectors below the time axis are the steering flow at 850 hPa (purple), 700 hPa (green), 500 hPa (red), and 300 hPa (blue) and the model's TC translation speed (black) from 0000 UTC 22 Aug to 25 Aug 2016 in the SM22 experiment.

FIG. 11. As in Fig. 10, but for the SM23 experiment.

evolution of the maximum wind speed (MWS) at the 10-m height in SM22, SM23, SM24 and the best track data from JTWC. Note that the initial intensities of all three simulations are weaker than the intensities in the best track. While the start times are different, the predicted trends of the intensity from the three simulations are similar, with all of them intensifying with time and the peaking time lags the observed. Figure 9 shows the vertical cross section of the *v*-component winds for SM22, SM23, and SM24 as differences in the initial intensity may lead to different vertical structures of the storm. Note that with different initial times, the comparison among the three needs to be lagged, with the 72-h prediction from SM22 and 48 h from SM23 to be compared with the 24-h prediction from SM24. With this consideration, all three simulated structures of the storm are similar. Based on this analysis, we conclude that the intensity differences play little role in the track differences for this case. The sensitivity of the storm intensity on its movement will be examined further in section 6.

To explore specific reasons behind the differences in TC tracks among these experiments, the time-vertical cross section of the steering flows in SM22, SM23, and SM24 are shown in Figs. 10–12, respectively. Compared with the steering flow in the observation (Fig. 5), the steering flow in SM22 has a mostly westerly component at all vertical levels between 0000 UTC 22 August and 0000 UTC 23 August (Fig. 10). The upper-level northerly steering in the next day is weaker than in the verifying analysis. The steering flow then turns more eastward after 0000 UTC 24 August, and is inconsistent with the observation. Meanwhile, while the upper-level flow weakens, the lower-level flow strengthens too early from
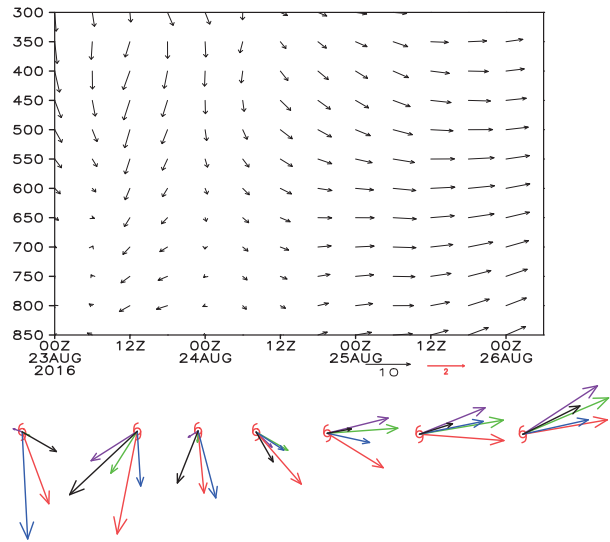
0000 UTC 24 August to 25 August in this simulation. Overall, the evolution of the steering vectors conforms well with the movement of the storm in the simulation and the early northeastward turn in SM22 is the result of weakening of the upper-level flow and development of lower-level westerly prematurely. Although the TC track in SM23 is better than that in SM22 as it starts with a stronger northerly flow on 23 August, the upper-level steering flow also changes from northerly to northwesterly prematurely (Fig. 11). As a result, the track of the TC in the SM23 experiment also takes an earlier turn before 0000 UTC 25 August. In the most accurate simulation for Lionrock starting on 24 August (SM24), the steering flow at upper levels remains toward the south at 1200 UTC 24 August (Fig. 12). At 0000 UTC 25 August, the upper-level steering turns to southwestward
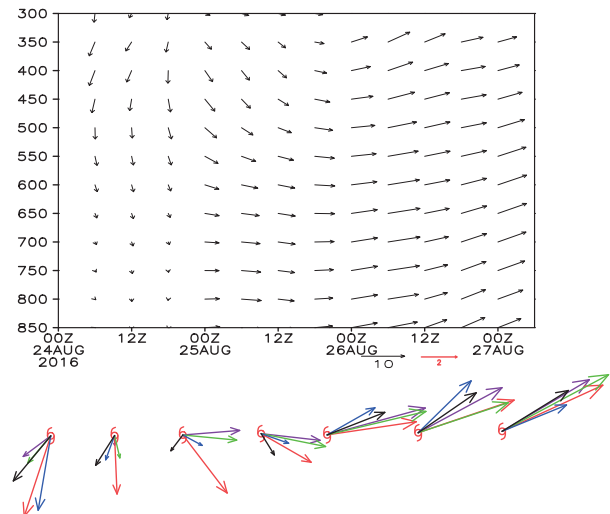

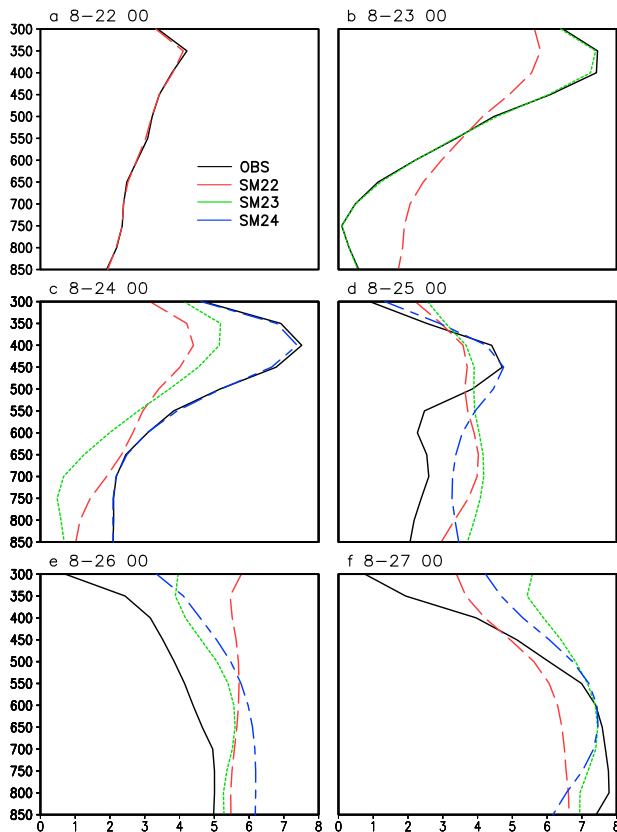FIG. 12. As in Fig. 10, but for the SM24 experiment.

FIG. 13. The vertical profiles of area-averaged (500 km × 500 km) magnitude of the steering flow (m s^{-1}) from the SM22 (red), SM23 (green), SM24 (blue) experiments, and observation (black).

and lower-level westerly steering starts precisely at this turning time as in the observation shown in Fig. 5.

Figure 13 shows the vertical profile of the steering magnitude of these experiments and from the reanalysis (replot of Fig. 6). This figure summaries the difference of the steering from the three simulations. The deviations of the vertical steering profiles from SM22 on 23 and 24 August are clear in Figs. 13b and 13c. The 1-day simulation from SM23 at 24 August shows a profile similar to the verification but with a smaller speed (green line in Fig. 13c). The vertical level of the maximum steering flow has moved downward from 450 hPa to near 700 hPa at 0000 UTC 25 August in both SM22 and SM23 (Fig. 13d). In other words, the shifting of maximum steer from the upper levels to the lower levels earlier than is observed has caused the TC to move to the northeast prematurely. The vertical profiles of the steering in SM24 (blue dashed lines) are more consistent with the observations and the simulated storm track is the best among the three experiments.

Figure 14 shows the time evolution of the simulated relative vorticity at 850 hPa and the wind field and the geopotential height at 500 hPa up to the turning point on 25 August, to be compared with the verifying reanalysis (Fig. 3). Note that while the wind fields at the initial time (Fig. 14a, 0000 UTC 22 August) and the NCEP reanalysis (Fig. 3a) are identical, the

geopotential contours are slightly different as the latter are derived in the model and depend on model levels and other parameters used in the hydrostatic approximation. The subtropical high split by Lionrock previously remains disconnected in the beginning in SM22 (Fig. 14a). The subtropical high system south of the storm becomes more connected between 23 and 24 August, inhibiting the southwestward movement of Lionrock (Figs. 14b,c), not consistent with the observation shown in Fig. 3. In SM23, a break in the subtropical high allows Lionrock continues to move to the southwest in the initial stage (Fig. 14e) until the subtropical high is re-established and limits Lionrock's farther southward movement on 24 August (Fig. 14f). The simulated fields of SM24 that starts on 24 August shows that the building of the subtropical high in the northwest is stronger and the southward flows along its eastern edge can steer Lionrock to the south (Figs. 14h,i). Additionally, the break in the subtropical ridge provides for Lionrock to move southward on 24 August (Fig. 14h), this is the reason why the storm continued its southward movement between 24 and 25 August and the northeastward turning point after 25 August is better simulated in SM24. The comparison between the numerical simulations and the observational analysis indicates that the southwest movement of the storm is related to the enhancement of the subtropical high in the WNP. When the western portion of the subtropical high develops stronger (Figs. 14a,e,h), the broken subtropical high is reconnected at a more exact time (on 25 August) (Figs. 14c,f,h), allowing the storm to continue moving southward before turning northeastward, which is closer to the Lionrock's observed motion.

Figure 15 shows the time evolution of the geopotential height, wind fields from the simulations and the difference of geopotential height between the observation and the simulations (shading), all at 300 hPa. The corresponding reanalysis in Fig. 4 shows that there is a trough in the midlatitudes on the northwest side of the storm. As Lionrock strengthens, the midlevel trough continues to extend southward (Fig. 4d). The trough simulated in SM22 is too shallow, as can be seen from the 9750-gpm line from 23 to 25 August (Figs. 15b–d), allowing the subtropical high to reconnect south of Lionrock and hinder its southward movement. The premature closure of the contour associated with the subtropical high implies a more westerly flow hinders the TC from continue moving southward on 24 August (Fig. 15c). This is also the reason why the upper-level steering flow in SM22 changes from northerly to northwesterly on 25 August prematurely (Fig. 10). In SM23, the 9750-gpm contour is connected south of Lionrock on 24 August, which generates a southwesterly flow to the right of the TC and accelerates the turning to the northeast (Fig. 15f). In SM24, the subtropical high is separated at the initial time (Fig. 15h). Compared with other two experiments, the closure of contour is delayed (Figs. 15c,f,i), and the upper-level westerly component of the flow appears later (Figs. 15h,i). In general, simulations on 24 August from the three simulations (Figs. 15c,f,h) tell the differences among them that impact the track of Lionrock. This is shown clearly in the vertical profiles of the steering speed in Fig. 13c in which SM22 and SM23 significantly underpredict the upper-level steering.
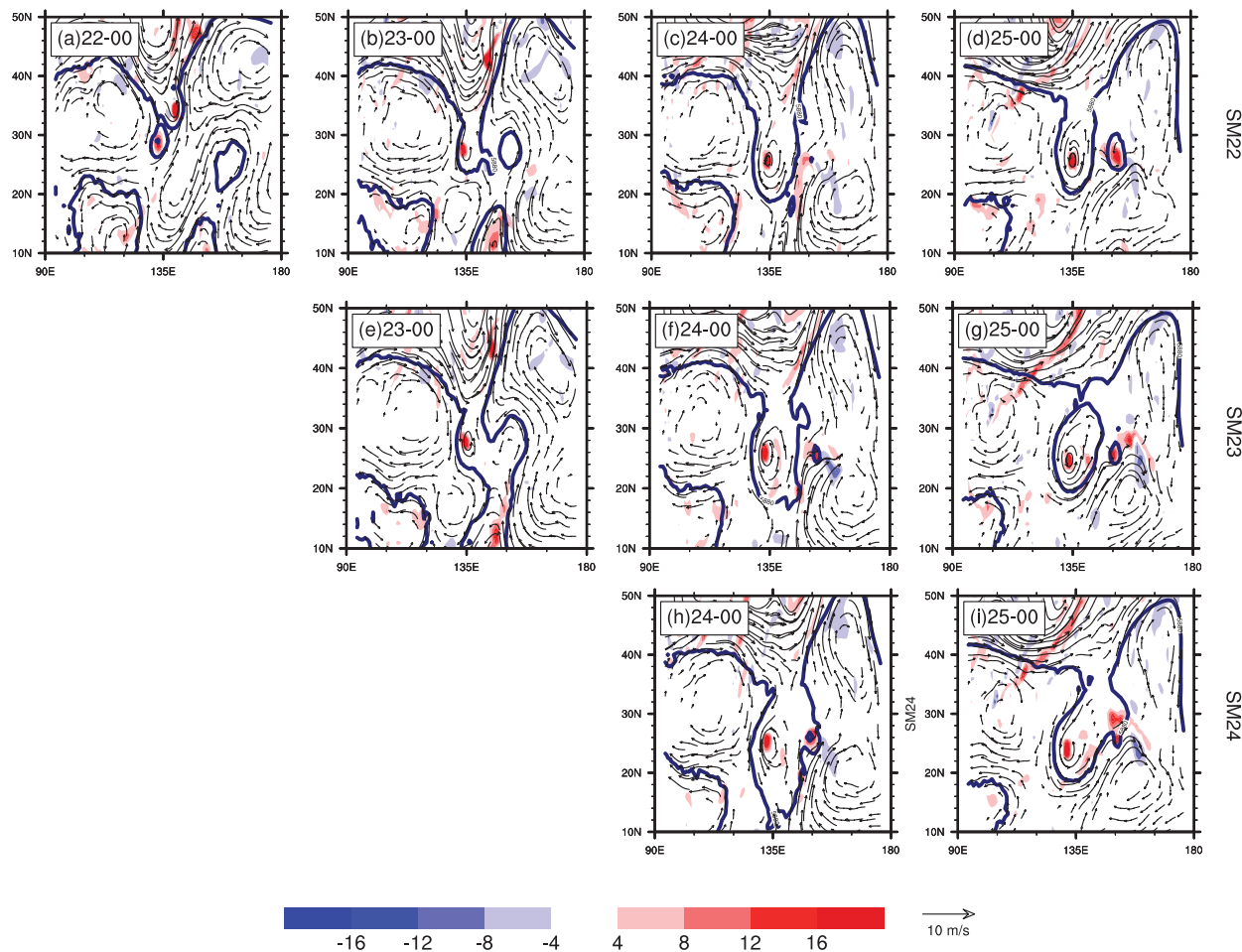
FIG. 14. As in Fig. 3, but for the (a)–(d) SM22, (e)–(g) SM23, and (h),(i) SM24 experiments.

Our previous discussion indicates that the characteristics of the subtropical high controls the southwest movement between 22 and 25 August and affect the turning of Lionrock. However, what causes Lionrock to loop back at the exact time as it did? Based on the discussion in section 4, Lionrock is steered by the low-level flow when it loops to the northeast. When the storm is about to make a significant turning starting around 25 August, the southwesterly wind to the south of Lionrock is rapidly increasing, causing Lionrock to move northeastward. Additionally, on 23 August, a monsoon gyre (MG; Lander 1994, 1996; Harr et al. 1996) develops to the northeast of Lionrock. To examine the evolution of the MG, the vertically integrated 10–60-day low-frequency circulation evolution was extracted from the NCEP FNL (Fig. 16) using a Lanczos filter (Duchon 1979). A black dot denotes the MG center (Lander 1994). On 23 August, Lionrock was located to the north of the MG center. Between 23 and 24 August, Lionrock moved southwest toward the MG center, and it arrived to the southwest of the MG by 25 August. Studies have shown that TC tracks are sensitive to the relative positions of the TC and a nearby MG (Carr and Elsberry 1995; Liang and Wu 2015). When the storm is

located on the western edge of the MG, the winds in the southern quadrant of the MG may cause Lionrock to undergo a looping motion. Although there is a significant difference in TC track among these three experiments, the timing of the track changes in SM23 and SM22 experiments is roughly one day ahead. In Fig. 17, the low-frequency mode simulated in the three experiments and the relative positions between Lionrock and the MG are compared. Following Bi et al. (2015), a 5-day running mean subtracted from a 30-day running mean is used instead of Lanczos filtering to extract the l0–60-day mode because of the data-coverage limitation in a regional model framework. At the initial time in SM22, Lionrock is located north of the MG center (Fig. 17a), but the two centers coincide temporally on 23 August without merging together. The storm reaches west of the MG on 24 August, and is steered by strong southwesterly winds on the southeastern edge of the MG to the northeast later on 24 August. This is more than one day earlier than in the reality. In SM23, there is a clear distance between Lionrock and the MG at the initial time (Fig. 17e) and the TC center arrives at the west side of the MG one day later than in SM22. The delay in the overlap of the two causes the storm to continue moving
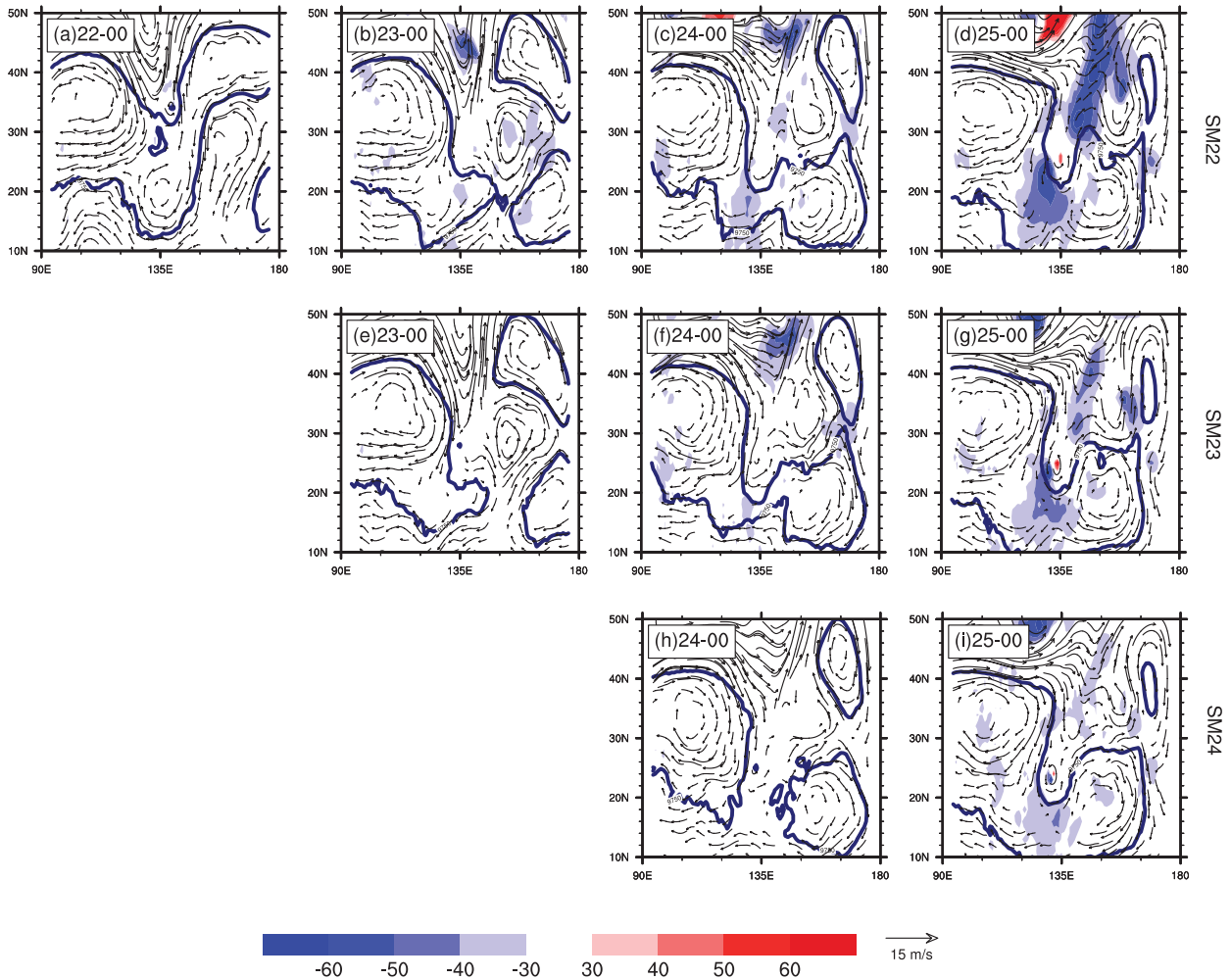
FIG. 15. The evolution of 9750-gpm geopotential height (contour) and wind vectors at 300 hPa and the difference of the geopotential height (shaded; gpm) between the observation and the (a)–(d) SM22, (e)–(g) SM23, and (h),(i) SM24 experiments.

southwest longer than in SM22 so that the simulated track in SM23 is better than in SM22 (Fig. 7). In SM24, the positions of Lionrock and the MG are separated at the initial time and the storm does not reach the west side of the MG until 25 August (Fig. 17i). The simulated track is most consistent with the best track. These three simulations suggest the track change of Lionrock is highly unpredictable.

Carr and Elsberry (2000) showed that errors in TC track forecasts are often associated with wind errors in the large-scale synoptic environment. Many studies have demonstrated the existence of Fujiwhara-type interactions between a TC and the MG (Carr and Elsberry 1995; Bi et al. 2015; Liang and Wu 2015; Ge et al. 2018). Our experiments indicate that the monsoon gyre, the dominant feature at the low level, interacts with the TC to provide the southwest steering flow for the looping of Lionrock toward northeast. In simulations of SM22 and SM23, incorrect relative positions between the storm and the MG cause their interactions to be ahead of the time. This causes the steering flow to shift prematurely from

high to low levels, and eventually results in the poor prediction of Lionrock's looping track.

To verify our hypothesis on the effect of the MG on the movement of Lionrock, an additional experiment starting on 0000 UTC 23 August is conducted in which the monsoon gyre is removed (NO_MG). The vortex-removing technique adopted in our study follows Kurihara et al. (1995). This method, used in the Geophysical Fluid Dynamics Laboratory (GFDL) hurricane prediction system (Kurihara et al. 1993, 1995) has been used widely in tropical cyclones related studies (i.e., Wu et al. 2002; Hsu et al. 2008). The setup of the prediction model is the same as in the other experiments except for the removal of the monsoon gyre. Figure 18 shows the track in the NO_MG experiment and the best track. Instead of the northeastward movement between 25 and 26 August, the TC in NO_MG moves southwest without turning. This result indicates that Lionrock's northeast turn is steered by the MG.

Figure 19 displays the evolution of the wind field at 850 hPa from 0000 UTC 23 August to 28 August, where there is evidence of Lionrock being embedded within the MG
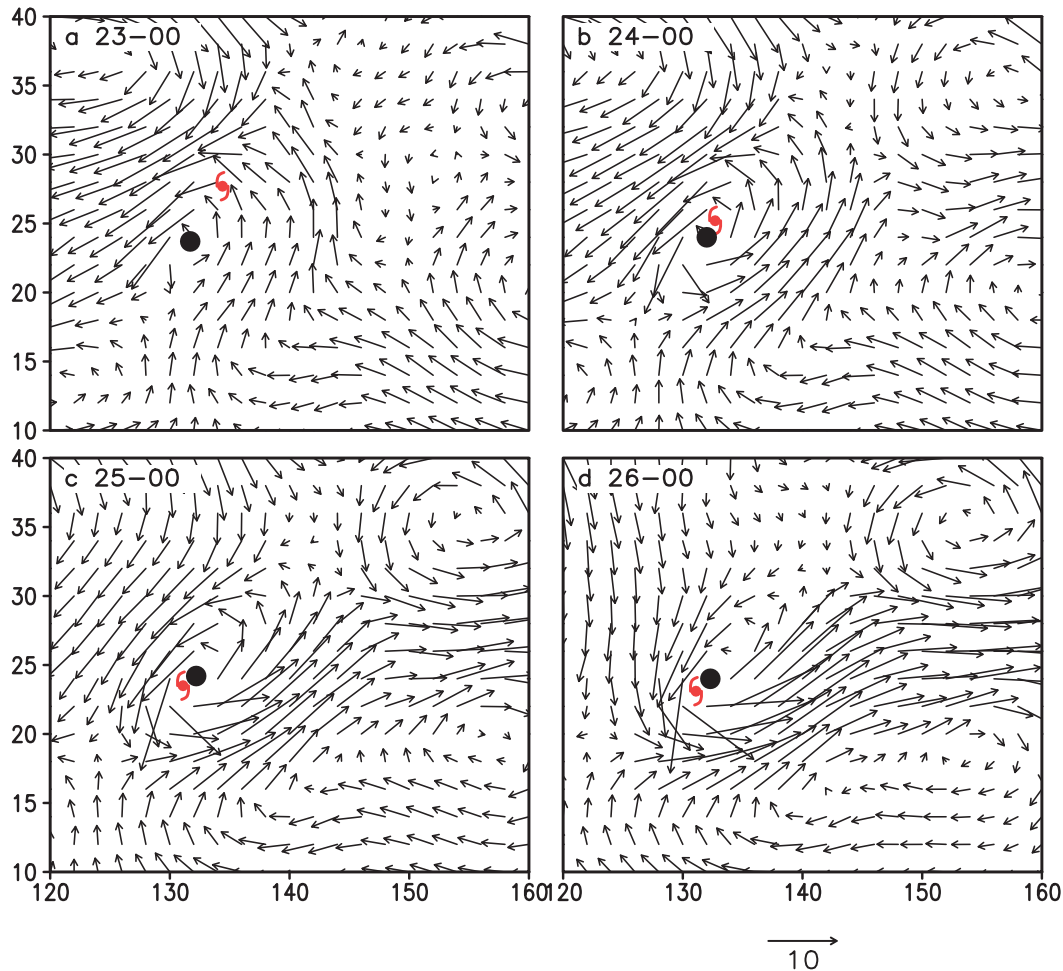
FIG. 16. The evolution of 10–60-day bandpass-filtered wind (vectors; m s^{-1}) averaged between 850 and 300 hPa from 23 to 26 Aug in the observation. The black dots and red typhoon symbols denote the centers of the low-frequency monsoon gyre and Lionrock, respectively.

circulation. Along with the development of Lionrock, the southwesterly flow in the southeastern portion of the MG gradually intensifies. A distinct high-wind region forms on the periphery of the southeast side of Lionrock on 26 August, and the region continues expanding and strengthening in subsequent days. This strong southwesterly flow pushes the tropical cyclone from its originally southwest direction to the northeast around 25 August. Previous studies found that during the coalescence of a TC with the MG, there will be a high-wind area similar to the monsoon surge due to the Rossby wave energy dispersion (Carr and Elsberry 1995; Ge et al. 2010). From the comparison between the observation and NO_MG experiment (Fig. 20), it can be seen that the winds surrounding the storm slow down, and the area of high winds is mostly concentrated near the TC center. Without the influence of strong southwesterly winds associated with the MG, the environmental flow at lower levels cannot steer Lionrock to loop northeastward.

In summary, analyzing the steering flows and the environmental flows at different levels sheds light on understanding

the unusual track of Lionrock (2016) for the period between 22 and 27 August. Our simulations starting at different initial time show that if the intensity and positions of the midlevel subtropical high and the upper-level trough are incorrectly represented, they will hinder the extent to which Lionrock can move southwest, leading to a northeast turn prematurely. Meanwhile, the main reason for the sudden northeastward turn of Lionrock is also due to its interaction with the nearby MG. When the storm reaches its farthest southwestern point, the southwesterly flow generated by the overlap of the MG and Lionrock starts pushing the TC northeastward. Therefore, the timing for the turn of Lionrock depends on the relative positions and interactions of the TC and the nearby MG. Errors in the predicted spatial relation between typhoon Lionrock and the MG result in the storm looping back prematurely.

6. Predictability of Lionrock

As revealed by the diversity of the predicted tracks of Lionrock by operational models (Fig. 2), the predictability of the
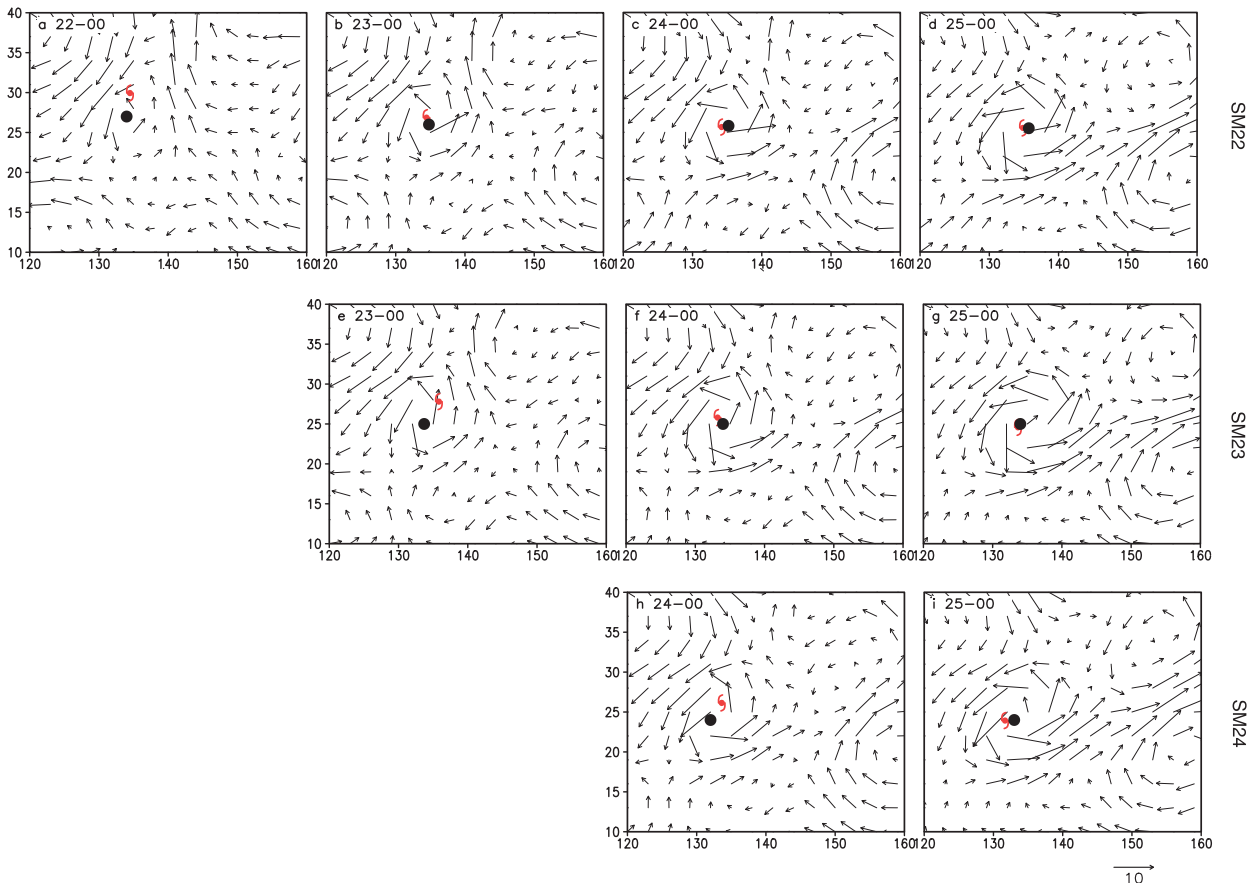
FIG. 17. As in Fig. 16, but for the (a)–(d) SM22, (e)–(g) SM23, and (h),(i) SM24 experiments.

track warrants more investigation. Since the SM22 experiment has the worst track prediction, we use this case as the base line to explore the predictability of the abrupt turn of Lionrock by modifying the initial and boundary conditions to obtain more uncertainties associated with the model integration. Since the turning position of Lionrock simulated by SM22 has a northeast bias, we first examine the sensitivity of the track to the TC's initial position by moving Lionrock 100 km west and south from its original position at the initial time on 22 August (identified as reloc_SM22). The Kurihara method (Kurihara et al. 1995), described in section 5, is used for the extraction and insertion of the TC vortex. The radius of the extraction is 450 km from the storm center to minimize its impact on the environment.

Second, as the simulated intensity of Lionrock in SM22 is too weak (Fig. 8), we ponder whether this weak intensity bias may limit interactions between Lionrock and its background flows, leading to a poor track prediction. To enhance the TC intensity, an idealized TC-like vortex with a maximum wind speed of 5 m s^{-1} at the radius of 100 km is constructed and superimposed on Lionrock's wind fields at all levels at the initial time on 22 August (inten_SM22). The wind speed of the synthetic vortex decreases with height to zero at 250 hPa. The mass and thermodynamic fields of it are derived based on

the nonlinear balance equation so that the vortex satisfies both the hydrostatic and gradient wind balances. More details of the synthetic vortex are discussed in Wang (1995, 2001). For these two experiments, the NCEP FNL reanalysis is used before modifications.

Figure 21 shows the simulated tracks and intensities from reloc_SM22, inten_SM22, the original SM22 experiment, and the best track. When the initial position of Lionrock is moved to the southwest, in the direction of the future movement, the overall simulated track also moves southwestward somewhat but the overall pattern of the new track remains similar to SM22 (Fig. 21a). The turning point also moves southwest compared with SM22, but the reloc_SM22 fails to produce the correct turning point. Meanwhile, changing the TC initial intensity also did not change the track significantly compared with SM22 (Fig. 21b). The TC intensity has been improved in inten_SM22, especially the maximum intensity (Fig. 21b). However, there is little impact on the track (Fig. 21a). The above two experiments indicate that the storm intensity and uncertainty of the initial position may not be strong factors in influencing the track. Our earlier analysis suggests that the large-scale environmental flow is important for Lionrock's track. To further demonstrate this point, the third additional experiment is conducted by using the European Centre for
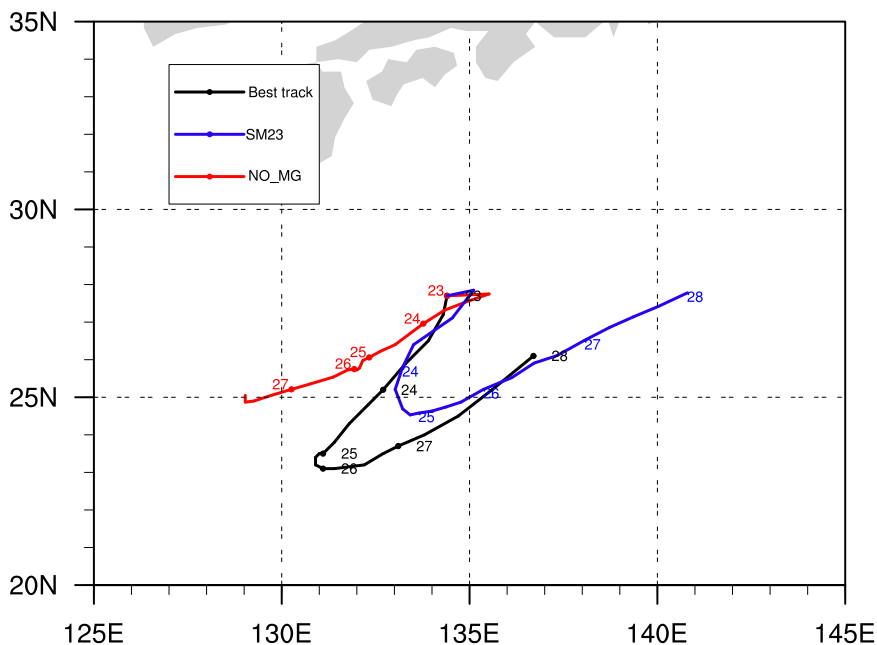
FIG. 18. The track of the TC in the NO_MG experiment (red), the SM23 experiment (blue), and the best track starting on 0000 UTC 23 Aug.

Medium-Range Weather Forecasts (ECMWF) reanalysis version 5 (ERA5) as the initial and boundary conditions (era_SM22). One of the reasons for choosing this analysis is that ERA5 has a higher resolution of 0.25° × 0.25° than the NCEP reanalysis of 1° × 1°. Higher resolution helps the prediction system to better represent the environment and thus may obtain a more accurate TC track. Figure 22 shows the track and evolution of the maximum wind speed in era_SM22 and the best track. With era_SM22, the simulated storm track has indeed been improved in its southwestward movement (Fig. 22a). However, the simulation of the turning point of Lionrock is still not perfect. This shows that in the later stage of the simulation, the environmental field was not simulated properly to steer Lionrock correctly. This is shown more clearly by the vertical profile of the steering speed in Fig. 23. At 23 and 24 August, the era_SM22 simulated steering is much better than the control SM22, especially the larger steering at high levels, leading to better simulated track during the first two days (Fig. 22a). At later stage, the steering from era_SM22 shows little improvement over SM22.

The vertical profiles of the steering flows for reloc_SM22 and inten_SM22 are also computed to obtain a quick view of the environment surrounding the storm from these simulations. Different from Fig. 23 for era_SM22, the steering flows for relocating the storm or increasing the storm intensity show little improvement over SM22 (figure not shown). In both experiments, the dominating steering flow at lower levels occurred prematurely, leading to an earlier turn of Lionrock.

It can be seen from Fig. 22b that the storm intensity is better simulated by using ERA analysis as the initial condition in era_SM22 and its evolution is very similar to the one in inten_SM22 where the initial storm intensity has been artificially enhanced. Note that there is no improvement of the track prediction in inten_SM22 over the original SM22 even though the intensity simulation has been improved. On the other hand, both the prediction of intensity and track of Lionrock have been improved in era_SM22. We attribute this to a more accurate environment in which the TC resided in era_SM22. This further suggests that the movement of Lionrock is mainly controlled by its environmental flow as indicates by the steering analysis.

As discussed before, the movement of Lionrock hinges on several different environmental features located at different levels at different time, rendering it less predictable. This series of new experiments reinforces our conclusion that when the initial moment of the simulation is pushed forward toward the critical turning time, the model will produce a more accurate large-scale environmental field, and the track of Lionrock will be more predictable. We speculate that this low predictability ties in with the change of the major steering in the vertical, namely, different controlling features in the environment.

7. Summary and discussion

Typhoon Lionrock, the tenth tropical cyclone in the western North Pacific in 2016, brought extensive disasters to Japan, South Korea, and eastern Russia. Most operational numerical models did poorly for Lionrock's unusual track. In this study, we investigate mechanisms for the sharp northeastward turn of Lionrock from its original southwestward movement at around 25 August. We analyze the time-
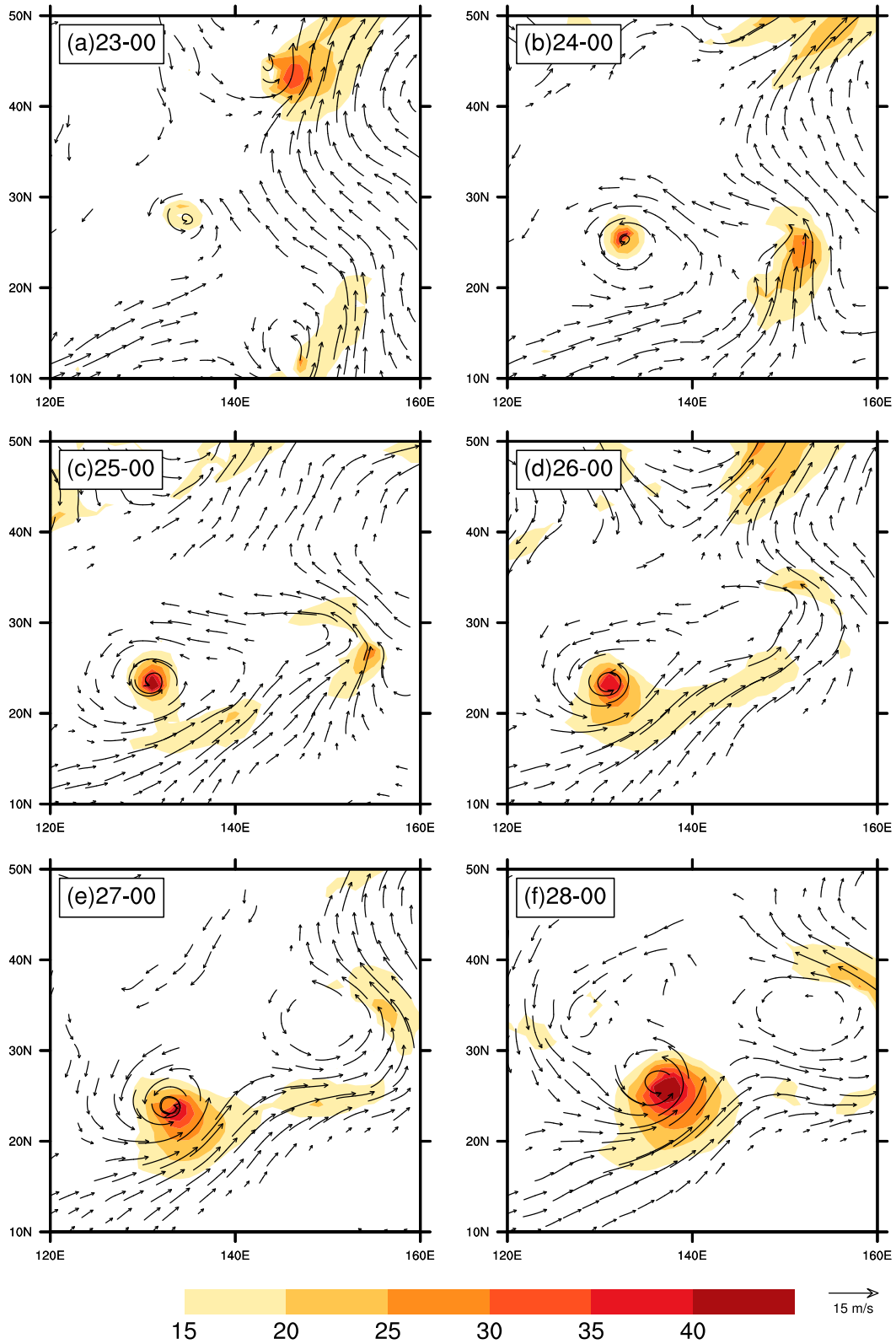
FIG. 19. The 850-hPa wind (vectors; m s^{-1}) and isotach (shaded; m s^{-1}) analyses from 0000 UTC (a) 23 Aug to (f) 28 Aug 2016 in NCEP reanalysis.
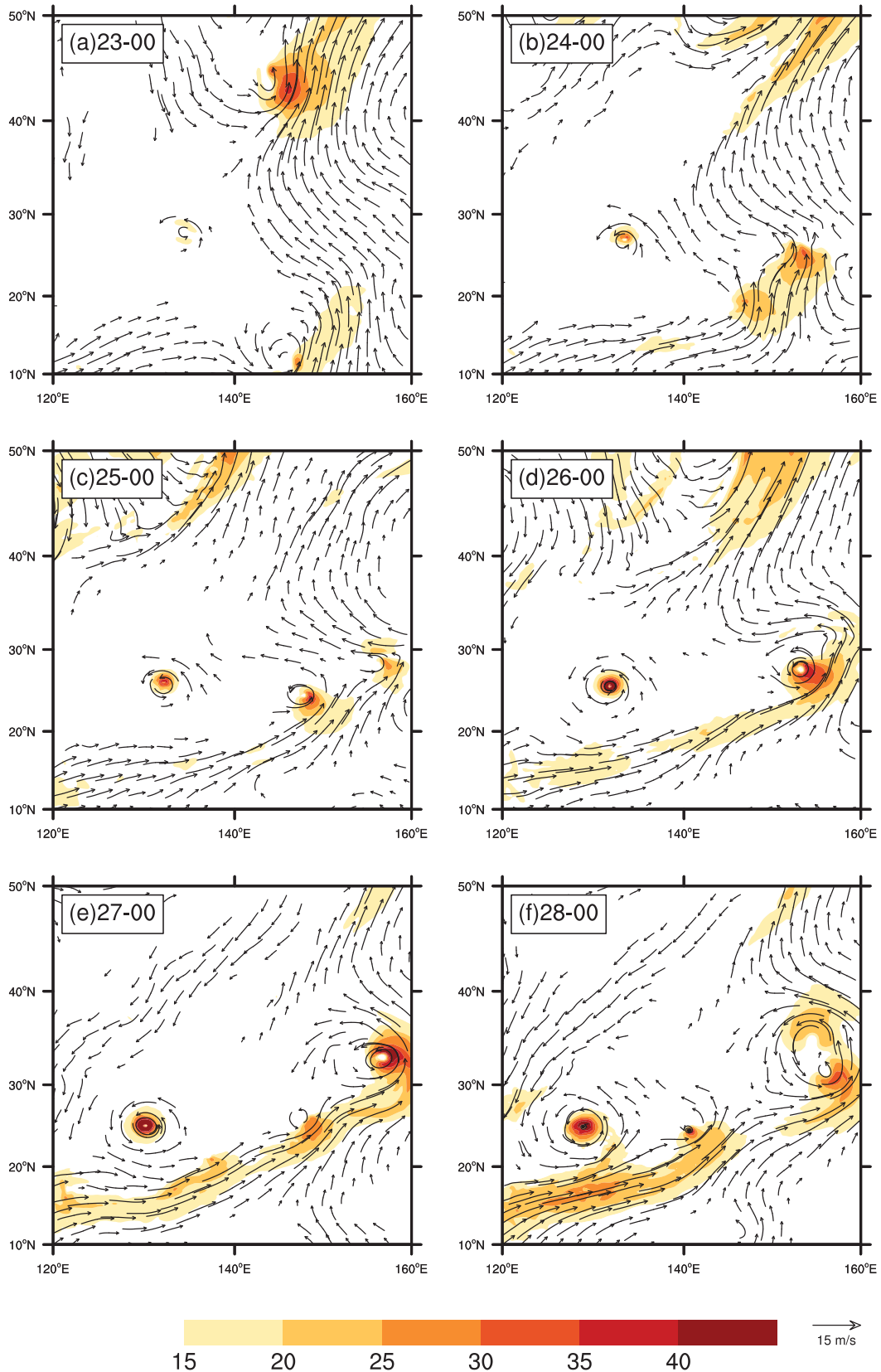
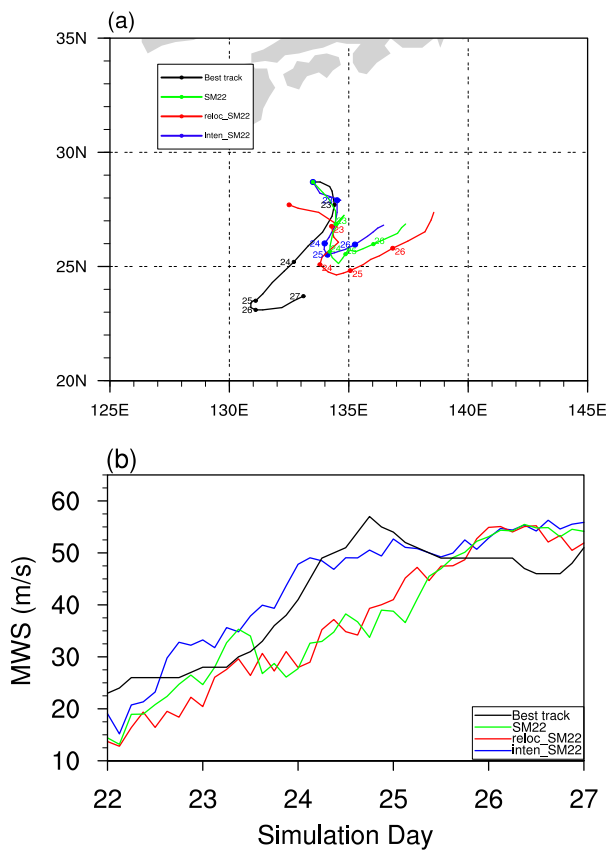FIG. 20. As in Fig. 19, but for the NO_MG experiments.

FIG. 21. (a) Time series of the MWS at 10-m height from the best track data (black) and SM22 (green), reloc_SM22 (red,) and inten_SM22 (blue). The x axis is the calendar day in August 2016. (b) The JTWC best track (black) of Lionrock and simulated tracks from SM22 (green), reloc_SM22 (red), and inten_SM22 (blue).

FIG. 22. As in Fig. 21, but for the era_SM22 (red) experiment.

vertical evolution of the steering flow within an area approximately 500 km from the center of the storm. The analysis indicates that Lionrock is mainly steered by the high-level flows during its southwest movement before it loops back to northeast when the dominant steering flow shifts to low levels.

To understand the reasons why Lionrock turned at the exact time it did, three numerical simulations are conducted using WRF Model and the NCEP FNL analysis as the initial and lateral boundary conditions. Our simulations starting 1, 2, and 3 days before the major turning point of Lionrock. In the simulation starting on 0000 UTC 22 August, three days before the turn, the simulated storm turns to the northeast too early and the turning point is too far from the actual track. The second simulation starts at 0000 UTC 23 August, and the model is able to simulate better the southwestward movement of Lionrock in the early stage followed by the northeast turning but the timing of the turn is also too early. In the third simulation starting at 0000 UTC 24 August, only one day ahead of the critical turn, the predicted track is closest to the real situation out of the three experiments. After analyzing the simulated results and the verifying reanalysis fields, it can be found
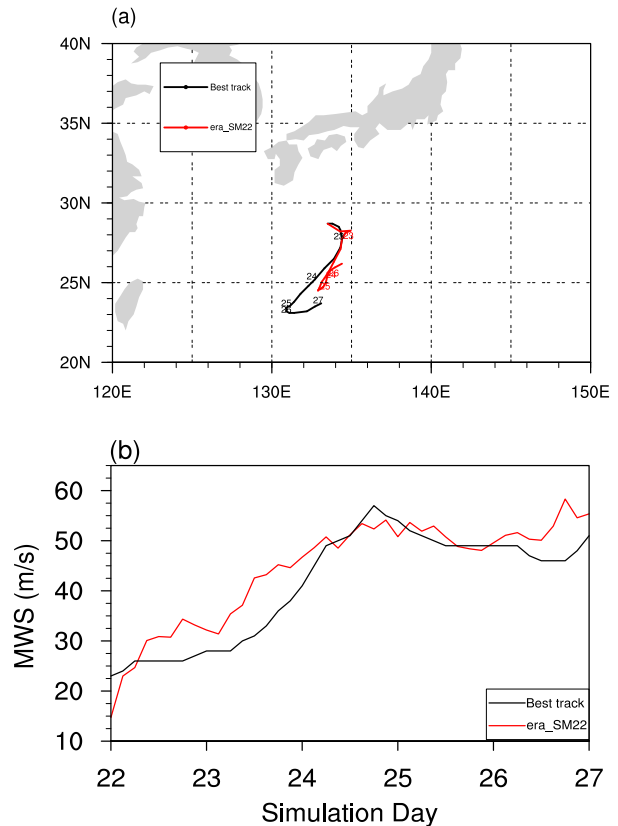
that the dominant level of the steering flow shifts from high to low levels at the turning point as reflected by the steering vectors at different levels. From the perspective of synoptic flows, the track of Lionrock before turning is primary controlled by the broken subtropical high and an upper-level trough, which leaves a north–south passage for Lionrock to move southwestward. Simulations of these mid- to upper-level synoptic systems determine how long Lionrock continued its southwestward movement. In the simulations that started earlier than 24 August, a westerly component of the wind due to the premature reconnection of two subtropical highs south of Lionrock limits the southward movement of the storm, causing the storm to turn northeastward too early. Based on the simulation results, errors in predicting the shift of the steering from the upper-level control to the lower-level control is the main reason for the failure of predicting the correct turning of Lionrock at the right time. The result suggests that an accurate TC track forecast requires proper representations of the large-scale environment.

In addition, Lionrock's looping to the northeast is caused by the lower-level southwesterly flow associated with a monsoon gyre interacting with Lionrock. To demonstrate the impact of the MG on Lionrock's northeast looping track, an additional experiment is conducted with the removal of the MG from the initial and boundary conditions. After eliminating the MG, Lionrock experiences a
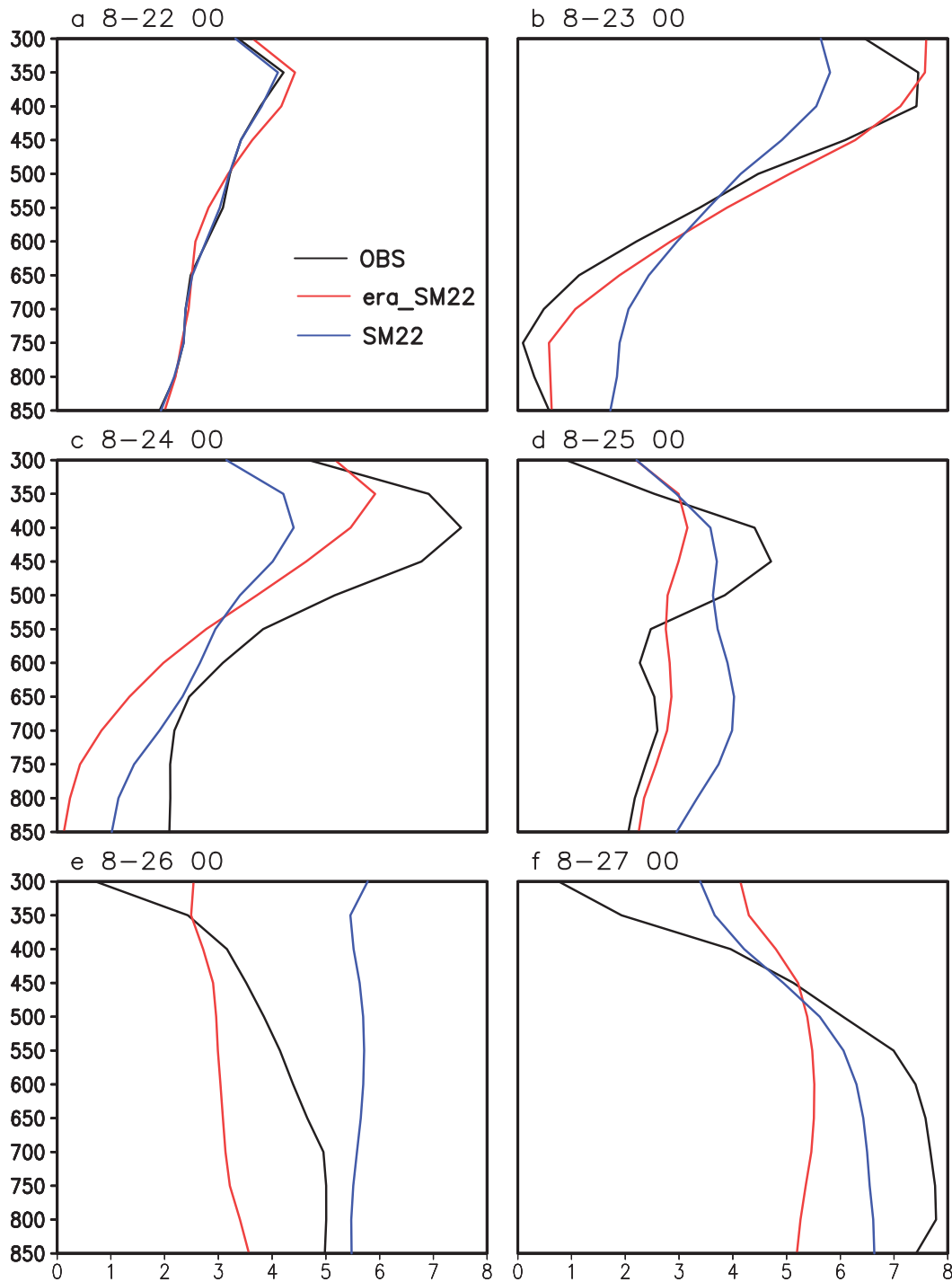
FIG. 23. As in Fig. 13, but for SM22 (blue) and era_SM22 (red).

continuous southwestward journey without looping back, which is different from the observation. This result suggests that the interaction between the storm and the MG plays a crucial role in Lionrock's northeastward turning at the precise time.

The predictability of Lionrock track is investigated using SM22 as the base line. First, two additional experiments are conducted by modifying the initial position and intensity of Lionrock with NCEP FNL reanalysis. When Lionrock is moved 100 km west and south from its original position in SM22, the pattern of the simulated track remains very similar to the track in SM22, as well as the intensity evolution. In the second sensitivity experiment, an idealized TC-like vortex

with a maximum wind speed of 5 m s^{-1} at the radius of 100 km is constructed and superimposed on Lionrock's analyzed structure at the initial time on 22 August to enhance Lionrock's initial intensity. The new experiment still failed to simulate the correct track, even though the intensity prediction was improved. The above two experiments suggest that the intensity of Lionrock and its initial position uncertainty have little effect on its track.

To further demonstrate that the large-scale environmental flows play a critical role in Lionrock movement, we conducted the third additional experiment using the ECMWF ERA5 reanalysis, which has a higher resolution, as the initial and boundary conditions. When the ECMWF reanalysis is used, the simulation does indeed improve Lionrock's southwestward movement. However, the simulated track still has room to improve in the later stage. When the initial time of the simulation is pushed forward, the uncertainty is reduced and the model can produce more accurate large-scale environmental fields and better track of Lionrock.

The results of the current study suggest that the low predictability of Lionrock ties in with the change of the major steering in the vertical. The failure in predicting Lionrock's abrupt northeastward turning at the critical time by many operational models may be due to inaccurate representation of shifting of the environmental control from the upper levels to the lower levels. More studies on unusual tracks and their associations with the steering flows will be conducted in the future.

Data availability statement. The reanalysis data were provided by the National Centers for Environmental Prediction (NCEP) final (FNL) analysis. The reanalysis data were provided by the European Centre for Medium-Range Weather Forecasts (ECMWF) reanalysis version 5 (ERA5). The data of Typhoon Lionrock was provided by the Joint Typhoon Warning Center (JTWC) (https://www.metoc.navy.mil/jtwc/jtwc.html). The real-time model forecasts are available at https://www.nrlmry.navy.mil/coamps-web/web/tc.

REFERENCES

Beljaars, A. C. M., 1994: The parameterization of surface fluxes in large-scale models under free convection. *Quart. J. Roy. Meteor. Soc.*, **121**, 255–270, https://doi.org/10.1002/qj.49712152203.

Bi, M., T. Li, M. Peng, and X. Shen, 2015: Interactions between Typhoon Megi (2010) and a low-frequency monsoon gyre. *J. Atmos. Sci.*, **72**, 2682–2702, https://doi.org/10.1175/JAS-D-14-0269.1.

Bosart, L. F., W. E. Bracken, J. Molinari, C. S. Velden, and P. G. Black, 2000: Environmental influences on the rapid intensification of Hurricane Opal (1995) over the Gulf of Mexico. *Mon. Wea. Rev.*, **128**, 322–352, https://doi.org/10.1175/1520-0493(2000)128<0322:EIOTRI>2.0.CO;2.

——, P. P. Papin, A. M. Bentley, and T. Burg, 2018: TC Lionrock (2016) touches all the bases during its lifecycle: Monsoon gyre, tropical transition, TC–TC interactions, a predecessor rain event, and extratropical transition. *33rd Conf. on Hurricanes and Tropical Meteorology*, Ponte Vedra, FL, Amer. Meteor. Soc., 1D.2, https://ams.confex.com/ams/33HURRICANE/webprogram/Paper339524.html.

Brand, S., 1970: Interaction of binary tropical cyclones of the western North Pacific Ocean. *J. Appl. Meteor.*, **9**, 433–441, https://doi.org/10.1175/1520-0450(1970)009<0433:IOBTCO>2.0.CO;2.

Carr, L. E., III, and R. L. Elsberry, 1990: Observational evidence for predictions of tropical cyclone propagation relative to environmental steering. *J. Atmos. Sci.*, **47**, 542–546, https://doi.org/10.1175/1520-0469(1990)047<0542:OEFPOT>2.0.CO;2.

——, and ——, 1995: Monsoonal interactions leading to sudden tropical cyclone track changes. *Mon. Wea. Rev.*, **123**, 265–290, https://doi.org/10.1175/1520-0493(1995)123<0265:MILTST>2.0.CO;2.

——, and ——, 1998: Objective diagnosis of binary tropical cyclone interactions for the western North Pacific basin. *Mon. Wea. Rev.*, **126**, 1734–1740, https://doi.org/10.1175/1520-0493(1998)126<1734:ODOBTC>2.0.CO;2.

——, and ——, 2000: Dynamical tropical cyclone track forecast errors. Part I: Tropical region error sources. *Wea. Forecasting*, **15**, 641–661, https://doi.org/10.1175/1520-0434(2000)015<0641:DTCTFE>2.0.CO;2.

Chan, J. C. L., and W. M. Gray, 1982: Tropical cyclone movement and surrounding flow relationships. *Mon. Wea. Rev.*, **110**, 1354–1374, https://doi.org/10.1175/1520-0493(1982)110<1354:TCMASF>2.0.CO;2.

Chang, C.-P., J. M. Chen, P. A. Harr, and L. E. Carr, 1996: Northwestward-propagating wave-like patterns over the tropical western North Pacific during summer. *Mon. Wea. Rev.*, **124**, 2245–2266, https://doi.org/10.1175/1520-0493(1996)124<2245:NPWPOT>2.0.CO;2.

Chen, J.-H., M. S. Peng, C. A. Reynolds, and C.-C. Wu, 2009: Interpretation of tropical cyclone forecast sensitivity from the singular vector perspective. *J. Atmos. Sci.*, **66**, 3383–3400, https://doi.org/10.1175/2009JAS3063.1.

Chen, T. C., S. Y. Wang, M. C. Yen, and A. J. Clark, 2009: Impact of the intraseasonal variability of the western North Pacific large-scale circulation on tropical cyclone tracks. *Wea. Forecasting*, **24**, 646–666, https://doi.org/10.1175/2008WAF2222186.1.

Davis, C. A., and L. F. Bosart, 2004: The TT problem: Forecasting the tropical transition of cyclones. *Bull. Amer. Meteor. Soc.*, **85**, 1657–1662, https://doi.org/10.1 175/BAMS-85-11-1657.

DeMaria, M., C. R. Sampson, J. A. Knaff, and K. D. Musgrave, 2014: Is tropical cyclone intensity guidance improving? *Bull. Amer. Meteor. Soc.*, **95**, 387–398, https://doi.org/10.1175/BAMS-D-12-00240.1.

Dong, K., and C. J. Neumann, 1983: On the relative motion of binary tropical cyclones. *Mon. Wea. Rev.*, **111**, 945–953, https://doi.org/10.1175/1520-0493(1983)111<0945:OTRMOB>2.0.CO;2.

Duchon, C. E., 1979: Lanczos filtering in one and two dimensions. *J. Appl. Meteor.*, **18**, 1016–1022, https://doi.org/10.1175/1520-0450(1979)018<1016:LFIOAT>2.0.CO;2.

Dudhia, J., 1989: Numerical study of convection observed during the Winter Monsoon Experiment using a mesoscale two-

dimensional model. *J. Atmos. Sci.*, **46**, 3077–3107, https://doi.org/10.1175/1520-0469(1989)046<3077:NSOCOD>2.0.CO;2.

Dzung, N. L., and T. J. Yamada, 2017: Simulation of tropical cyclone 201610 (Lionrock) and its remote effect on heavy rainfall in Hokkaido. *J. Japan Soc. Civ. Eng.*, **73**, 199–204, https://doi.org/10.2208/jscejhe.73.I_199.

Fiorino, M., and R. L. Elsberry, 1989: Some aspects of vortex structure related to tropical cyclone motion. *J. Atmos. Sci.*, **46**, 975–990, https://doi.org/10.1175/1520-0469(1989)046<0975:SAOVSR>2.0.CO;2.

Fujiwhara, S., 1921: The mutual tendency toward symmetry of motion and its application as a principle in meteorology. *Quart. J. Roy. Meteor. Soc.*, **47**, 287–292, https://doi.org/10.1002/qj.49704720010.

——, 1923: On the growth and decay of vortical systems. *Quart. J. Roy. Meteor. Soc.*, **49**, 75–104, https://doi.org/10.1002/qj.49704920602.

Ge, X., T. Li, S. Zhang, and M. Peng, 2010: What causes the extremely heavy rainfall in Taiwan during Typhoon Morakot (2009)? *Atmos. Sci. Lett.*, **11**, 46–50, https://doi.org/10.1002/asl.255.

——, Z. Yan, M. S. Peng, M. Bi, and T. Li, 2018: Sensitivity of tropical cyclone track to the vertical structure of a nearby monsoon gyre. *J. Atmos. Sci.*, **75**, 2017–2028, https://doi.org/10.1175/JAS-D-17-0201.1.

George, J. E., and W. M. Gray, 1976: Tropical cyclone motion and surrounding parameter relationships. *J. Appl. Meteor.*, **15**, 1252–1264, https://doi.org/10.1175/1520-0450(1976)015<1252:TCMASP>2.0.CO;2.

Hanley, D., J. Molinari, and D. Keyser, 2001: A composite study of the interactions between tropical cyclones and upper-tropospheric troughs. *Mon. Wea. Rev.*, **129**, 2570–2584, https://doi.org/10.1175/1520-0493(2001)129<2570:ACSOTI>2.0.CO;2.

Harr, P. A., and R. L. Elsberry, 1991: Tropical cyclone track characteristics as a function of large-scale circulation anomalies. *Mon. Wea. Rev.*, **119**, 1448–1468, https://doi.org/10.1175/1520-0493(1991)119<1448:TCTCAA>2.0.CO;2.

——, ——, and J. C. L. Chan, 1996: Transformation of a large monsoon depression to a tropical storm during TCM-93. *Mon. Wea. Rev.*, **124**, 2625–2643, https://doi.org/10.1175/1520-0493(1996)124<2625:TOALMD>2.0.CO;2.

——, ——, and T. F. Hogan, 2000: Extratropical transition of tropical cyclones over the western North Pacific. Part II: The impact of midlatitude circulation characteristics. *Mon. Wea. Rev.*, **128**, 2634–2653, https://doi.org/10.1175/1520-0493(2000)128<2634:ETOTCO>2.0.CO;2.

Holland, G. J., 1983: Tropical cyclone motion: Environmental interaction plus a beta effect. *J. Atmos. Sci.*, **40**, 328–342, https://doi.org/10.1175/1520-0469(1983)040<0328:TCMEIP>2.0.CO;2.

——, 1984: Tropical cyclone motion: A comparison of theory and observation. *J. Atmos. Sci.*, **41**, 68–75, https://doi.org/10.1175/1520-0469(1984)041<0068:TCMACO>2.0.CO;2.

Hong, S.-Y., and J.-O. J. Lim, 2006: The WRF single-moment 6-class microphysics scheme (WSM6). *J. Korean Meteor. Soc.*, **42**, 129–151.

——, Y. Noh, and J. Dudhia, 2006: A new vertical diffusion package with an explicit treatment of entrainment processes. *Mon. Wea. Rev.*, **134**, 2318–2341, https://doi.org/10.1175/MWR3199.1.

Hsu, H.-H., C.-H. Hung, A.-K. Lo, C.-C. Wu, and C.-W. Hung, 2008: Influence of tropical cyclones on the estimation of

climate variability in the tropical western North Pacific. *J. Climate*, **21**, 2960–2975, https://doi.org/10.1175/2007JCLI1847.1.

Kain, J. S., and J. M. Fritsch, 1993: Convective parameterization for mesoscale models: The Kain–Fritsch scheme. *The Representation of Cumulus Convection in Numerical Models*, *Meteor. Monogr.*, No. 46, Amer. Meteor. Soc., 165–170.

Kalnay, E., and Coauthors, 1996: The NCEP/NCAR 40-Year Reanalysis Project. *Bull. Amer. Meteor. Soc.*, **77**, 437–471, https://doi.org/10.1175/1520-0477(1996)077<0437:TNYRP>2.0.CO;2.

Kasahara, A., 1957: The numerical prediction of hurricane movement with the barotropic model. *J. Atmos. Sci.*, **14**, 386–402, https://doi.org/10.1175/1520-0469(1957)014<0386:TNPOHM>2.0.CO;2.

——, 1960: The numerical prediction of hurricane movement with a two-level baroclinic model. *J. Atmos. Sci.*, **17**, 357–370, https://doi.org/10.1175/1520-0469(1960)017<0357:TNPOHM>2.0.CO;2.

Kurihara, Y., M. A. Bender, and R. J. Ross, 1993: An initialization scheme of hurricane models by vortex specification. *Mon. Wea. Rev.*, **121**, 2030–2045, https://doi.org/10.1175/1520-0493(1993)121<2030:AISOHM>2.0.CO;2.

——, ——, R. E. Tuleya, and R. J. Ross, 1995: Improvements in the GFDL hurricane prediction system. *Mon. Wea. Rev.*, **123**, 2791–2801, https://doi.org/10.1175/1520-0493(1995)123<2791:IITGHP>2.0.CO;2.

Lander, M. A., 1994: Description of a monsoon gyre and its effects on the tropical cyclones in the western North Pacific during August 1991. *Wea. Forecasting*, **9**, 640–654, https://doi.org/10.1175/1520-0434(1994)009<0640:DOAMGA>2.0.CO;2.

——, 1996: Specific tropical cyclone track types and unusual tropical cyclone motions associated with a reverse-oriented monsoon trough in the western North Pacific. *Wea. Forecasting*, **11**, 170–186, https://doi.org/10.1175/1520-0434(1996)011<0170:STCTTA>2.0.CO;2.

——, and G. J. Holland, 1993: On the interaction of tropical-cyclone-scale vortices. I: Observations. *Quart. J. Roy. Meteor. Soc.*, **119**, 1347–1361, https://doi.org/10.1002/qj.49711951406.

Lau, K.-H., and N.-C. Lau, 1990: Observed structure and propagation characteristics of tropical summertime synoptic scale disturbances. *Mon. Wea. Rev.*, **118**, 1888–1913, https://doi.org/10.1175/1520-0493(1990)118<1888:OSAPCO>2.0.CO;2.

——, and ——, 1992: The energetics and propagation dynamics of tropical summertime synoptic-scale disturbances. *Mon. Wea. Rev.*, **120**, 2523–2539, https://doi.org/10.1175/1520-0493(1992)120<2523:TEAPDO>2.0.CO;2.

Lee, T.-C., T. R. Knutson, H. Kamahori, and M. Ying, 2012: Impacts of climate change on tropical cyclones in the western North Pacific basin. Part I: Past observations. *Trop. Cyclone Res. Rev.*, **1**, 213–230, https://doi.org/10.6057/2012TCRR02.08.

Li, T., and P.-C. Hsu, 2018: *Fundamentals of Tropical Climate Dynamics.* Springer, 239 pp.

Liang, J., and L. Wu, 2015: Sudden track changes of tropical cyclones in monsoon gyres: Full-physics, idealized numerical experiments. *J. Atmos. Sci.*, **72**, 1307–1322, https://doi.org/10.1175/JAS-D-13-0393.1.

——, ——, X. Ge, and C.-C. Wu, 2011: Monsoonal influence on Typhoon Morakot (2009). Part II: Numerical study. *J. Atmos. Sci.*, **68**, 2222–2235, https://doi.org/10.1175/2011JAS3731.1.

Mlawer, E. J., S. J. Taubman, P. D. Brown, M. J. Iacono, and S. A. Clough, 1997: Radiative transfer for inhomogeneous atmospheres: RRTM, a validated correlated–k model for the

longwave. *J. Geophys. Res.*, **102**, 16663–16682, https://doi.org/10.1029/97JD00237.

Peng, M. S., R. N. Maue, C. A. Reynolds, and R. H. Langland, 2007: Hurricanes Ivan, Jeanne, Karl (2004) and mid-latitude trough interactions. *Meteor. Atmos. Phys.*, **97**, 221–237, https://doi.org/10.1007/s00703-006-0254-z.

Podlaha, A., S. Bowen, C. Darbinyan, and M. Lorinc, 2016: Global Catastrophe Recap, October 2016. Aon Benfield Tech. Rep., 18 pp., http://thoughtleadership.aonbenfield.com/Documents/20161109-ab-analytics-if-october-global-recap.pdf.

Skamarock, W. C., and Coauthors, 2008: A description of the Advance Research WRF version 3. NCAR Tech. Note NCAR/TN-475+STR, 113 pp., https://doi.org/10.5065/D68S4MVH.

Straub, K. H., and G. N. Kiladis, 2003: Interactions between the boreal summer intraseasonal oscillation and higher-frequency tropical wave activity. *Mon. Wea. Rev.*, **131**, 945–960, https://doi.org/10.1175/1520-0493(2003)131<0945:IBTBSI>2.0.CO;2.

Sun, Y., Z. Zhong, L. Yi, T. Li, M. Chen, H. Wan, Y. Wang, and K. Zhong, 2015: Dependence of the relationship between the tropical cyclone track and western Pacific subtropical high intensity on initial storm size: A numerical investigation. *J. Geophys. Res. Atmos.*, **120**, 11451–11467, https://doi.org/10.1002/2015JD023716.

Tewari, M., and Coauthors, 2004: Implementation and verification of the unified NOAH land surface model in the WRF model. *20th Conf. on Weather Analysis and Forecasting/16th Conf. on Numerical Weather Prediction*, Seattle, WA, Amer. Meteor. Soc., 11–15.

Torn, R. D., T. J. Elless, P. P. Papin, and C. A. Davis, 2018: Tropical cyclone track sensitivity in deformation steering flow. *Mon. Wea. Rev.*, **146**, 3183–3201, https://doi.org/10.1175/MWR-D-18-0153.1.

Velden, C., and L. Leslie, 1991: The basic relationship between tropical cyclone intensity and the depth of the environmental steering layer in the Australian region. *Wea. Forecasting*, **6**, 244–253, https://doi.org/10.1175/1520-0434(1991)006<0244:TBRBTC>2.0.CO;2.

Wada, A., and R. Oyama, 2018: Relation of convective bursts to changes in the intensity of Typhoon Lionrock (2016) during the decay phase simulated by an atmosphere-wave-ocean coupled model. *J. Meteor. Soc. Japan*, **96**, 489–509, https://doi.org/10.2151/jmsj.2018-052.

Wang, Y. Q., 1995: On an inverse balance equation in sigma coordinates for model initialization. *Mon. Wea. Rev.*, **123**, 482–488, https://doi.org/10.1175/1520-0493(1995)123<0482:AIBEIS>2.0.CO;2.

——, 2001: An explicit simulation of tropical cyclones with a triply nested movable mesh primitive equation model: TCM3. Part I: Model description and control experiment. *Mon. Wea. Rev.*, **129**, 1370–1394, https://doi.org/10.1175/1520-0493(2001)129<1370:AESOTC>2.0.CO;2.

Wu, C.-C., and K. A. Emanuel, 1995a: Potential vorticity diagnostics of hurricane movement. Part I: A case study of Hurricane Bob (1991). *Mon. Wea. Rev.*, **123**, 69–92, https://doi.org/10.1175/1520-0493(1995)123<0069:PVDOHM>2.0.CO;2.

——, and ——, 1995b: Potential vorticity diagnostics of hurricane movement. Part II: Tropical Storm Ana (1991) and Hurricane Andrew (1992). *Mon. Wea. Rev.*, **123**, 93–109, https://doi.org/10.1175/1520-0493(1995)123<0093:PVDOHM>2.0.CO;2.

——, T.-H. Yen, Y.-H. Kuo, and W. Wang, 2002: Rainfall simulation associated with Typhoon Herb (1996) near Taiwan. Part I: The topographic effect. *Wea. Forecasting*, **17**, 1001–1015, https://doi.org/10.1175/1520-0434(2003)017<1001:RSAWTH>2.0.CO;2.

——, J.-H. Chen, P.-H. Lin, and K.-H. Chou, 2007: Targeted observations of tropical cyclone movement based on the adjoint derived sensitivity steering vector. *J. Atmos. Sci.*, **64**, 2611–2626, https://doi.org/10.1175/JAS3974.1.

——, S.-G. Chen, J.-H. Chen, K.-H. Chou, and P.-H. Lin, 2009: Interaction of Typhoon Shanshan (2006) with the midlatitude trough from both adjoint-derived sensitivity steering vector and potential vorticity perspectives. *Mon. Wea. Rev.*, **137**, 852–862, https://doi.org/10.1175/2008MWR2585.1.

Wu, L., and B. Wang, 2000: A potential vorticity tendency diagnostic approach for tropical cyclone motion. *Mon. Wea. Rev.*, **128**, 1899–1911, https://doi.org/10.1175/1520-0493(2000)128<1899:APVTDA>2.0.CO;2.

Yang, L., Y. Du, D. Wang, C. Wang, and X. Wang, 2015: Impact of intraseasonal oscillation on the tropical cyclone track in the South China Sea. *Climate Dyn.*, **44**, 1505–1519, https://doi.org/10.1007/s00382-014-2180-y.